2:00 pm: **In vivo imaging with GRIN-lens optical resolution photoacoustic micro-endoscopy**, Parsin Hajireza, Wei Shi, Peng Shao, Alexander Forbrich, Roger J. Zemp, Univ. of Alberta (Canada) . . . . . [8223-17]

2:15 pm: **Photoacoustic ophthalmology in mouse eyes**, Wei Song, Northwestern Univ. (USA); Shuliang Jiao, The Univ. of Southern California (USA); Hao F. Zhang, Northwestern Univ. (USA) . . . . . [8223-18]

2:30 pm: **Optoacoustic 3D visualization of changes in physiological properties of mouse tissues from live to postmortem**, Richard Su, Sergey Ermiliov, Anton Liopo, Vyacheslav Nadvoretsky, Travis Hernandez, Alexander A. Oraevsky, TomoWave Labs., Inc. (USA) . . . . . [8223-19]

2:45 pm: **Photoacoustic tomography of the monkey brain using virtual point detectors: experiment**, Liming Nie, Chao Huang, Zijian Guo, Mark A. Anastasio, Lihong V. Wang, Washington Univ. in St. Louis (USA) . . . . . [8223-20]

Coffee Break . . . . . 3:00 to 3:30 pm

SESSION 4

Room: 305 (Esplanade) . . . . . Sun. 3:30 to 5:45 pm

Quantitative Imaging and Measurements

Session Chairs: **Paul Beard,** Univ. College London (United Kingdom); **Rinat O. Esenaliev,** The Univ. of Texas Medical Branch (USA)

3:30 pm: **In vivo functional and molecular photoacoustic imaging of endogenous and exogenous chromophores using quantitative spectroscopic techniques**, Jan G. Laufer, Benjamin T. Cox, Univ. College London (United Kingdom); Bradley E. Treeby, The Australian National Univ. (Australia); Edward Zhang, Paul Beard, Univ. College London (United Kingdom) . . . . . [8223-21]

3:45 pm: **Functional photoacoustic microscopy of pH**, Muhammad R. Chatni, Junjie Yao, Amos Danielli, Christopher P. Favazza, Konstantin I. Maslov, Lihong V. Wang, Washington Univ. in St. Louis (USA) . . . . . [8223-22]

4:00 pm: **Photoacoustic correlation spectroscopy for in vivo blood flow speed measurement**, Sung-Liang Chen, Univ. of Michigan (USA); Zhixing Xie, Paul L. Carson, Xueding Wang, Univ. of Michigan Medical School (USA); L. Jay Guo, Univ. of Michigan (USA) . . . . . [8223-23]

4:15 pm: **Blood flow measurements using a pulsed time correlation photoacoustic Doppler technique: accuracy, resolution, and velocity range**, Joanna Brunker, Paul Beard, Univ. College London (United Kingdom) . [8223-24]

4:30 pm: **Investigations into soft tissue discrimination obtainable in thermoacoustic imaging**, Olumide Ogunlade, Paul Brennan, Paul Beard, Univ. College London (United Kingdom) . . . . . [8223-25]

4:45 pm: **In vivo imaging of inducible tyrosinase gene expression with an ultrasound array-based photoacoustic system**, Tyler Harrison, Robert J. Paproski, Roger J. Zemp, Univ. of Alberta (Canada) . . . . . [8223-26]

5:00 pm: **Temperature mapping using photoacoustic and thermoacoustic tomography**, Haixin Ke, Washington Univ. in St. Louis (USA); Todd N. Erpelding, Ladislav Jankovic, Philips Research North America (USA); Lihong V. Wang, Washington Univ. in St. Louis (USA) . . . . . [8223-27]

5:15 pm: **In vivo photoacoustic tomography of total blood flow and Doppler angle**, Junjie Yao, Konstantin I. Maslov, Lihong V. Wang, Washington Univ. in St. Louis (USA) . . . . . [8223-28]

5:30 pm: **Hemoglobin oxygen saturation measurement in rat retinal vessels by multiwavelength laser-scanning photoacoustic ophthalmoscopy,** Qing Wei, Northwestern Univ. (USA); Shuliang Jiao, The Univ. of Southern California (USA); Hao F. Zhang, Northwestern Univ. (USA) . . . . . [8223-29]

POSTERS - SUNDAY

Room: 103 (Exhibit Level) . . . . . Sun. 5:30 to 7:30 pm

Conference attendees are invited to attend the BiOS poster session on Sunday evening. Come view the posters, enjoy light refreshments, ask questions, and network with colleagues in your field. Authors of poster papers will be present to answer questions concerning their papers. Attendees are required to wear their conference registration badges to the poster sessions. Poster authors, view poster presentation guidelines and set-up instructions at http://spie.org/x27476.xml.

Compact fiber-Bragg-grating detector for high-sensitivity ultrasound measurements, Amir Rosenthal, Daniel Razansky, Vasilis Ntziachristos, Helmholtz Zentrum München GmbH (Germany) . . . . . [8223-81]

The study of quantitative optical absorption imaging by using Monte Carlo simulation of combined photoacoustic tomography and ultrasound-modulated optical tomography, Chulhong Kim, Yang Li, Univ. at Buffalo (USA); Lihong V. Wang, Washington Univ. in St. Louis (USA) . . . . . [8223-82]

A method for simultaneously estimating acoustic and optical properties of heterogeneous absorber using focused photoacoustic imaging based on Hilbert transform, Zhifang Li, Zhiping Zeng, Hui Li, Fujian Normal Univ. (China) . . . . . [8223-83]

3D digital acousto-optical coherence tomography, Emilie Benoit, Salma Farahi, Emmanuel Bossy, Francois Ramaz, Ecole Supérieure de Physique et de Chimie Industrielles (France) . . . . . [8223-84]

Photoacoustic spectral characterization of liquid perfluorocarbon droplets, Eric Strohm, Min Rui, Ryerson Univ. (Canada); Ivan Gorelikov, Naomi Matsuura, Sunnybrook Health Sciences Ctr. (Canada); Michael C. Kolios, Ryerson Univ. (Canada) . . . . . [8223-85]

Photoacoustic microscopy of myocardial sheet architecture in unfixed and unstained mammalian hearts, Chi Zhang, Ya-Jian Cheng, Da-Kang Yao, Washington Univ. in St. Louis (USA); Samuel A. Wickline M.D., Washington Univ. School of Medicine in St. Louis (USA); Lihong V. Wang, Washington Univ. in St. Louis (USA) . . . . . [8223-86]

Photoacoustic sensing of exogeneously delivered contrast agents using high-frequency ultrasonic transducers, Pavel V. Subochev, Roman V. Belyaev, Aleksey R. Katichev, Andrey N. Morozov, Anna G. Orlova, Ilya V. Turchin, Institute of Applied Physics (Russian Federation) . . . . . [8223-87]

Developing a stochastic model for acousto-optic tissue imaging, Steffen G. Resink, Wiendelt Steenbergen, MIRA Institute for Biomedical Technology and Technical Medicine (Netherlands) . . . . . [8223-88]

Measuring tissue blood flow using ultrasound modulated diffused light: a preclinical study, Ilan Breskin, Avihai Ron, Noam Racheli, Coby Metzger M.D., Zmira Silman, Moshe Kamar M.D., Asaph Nini M.D., Michal Balberg, Revital Shechter, Ornim Medical Ltd. (Israel) . . . . . [8223-89]

Drug delivery monitoring by photoacoustic tomography with an ICG encapsulated double emulsion, Xueding Wang, Justin Rajian, Mario Fabiilli, J. Brian Fowlkes, Paul L. Carson, Univ. of Michigan Medical School (USA) . . . . . [8223-90]

An optical resolution photoacoustic dermoscope for port-wine stain imaging, Bin Rao, Washington Univ. in St. Louis (USA); Wangcun Jia, J. Stuart Nelson, Beckman Laser Institute and Medical Clinic (USA); Lihong V. Wang, Washington Univ. in St. Louis (USA) . . . . . [8223-91]

Photoacoustic speckles: boundary dependence and experimental validation, Zijian Guo, Zhun Xu, Lihong V. Wang, Washington Univ. in St. Louis (USA) . . . . . [8223-92]

Photoacoustic molecular imaging on ferritin as a reporter gene, Seunghan Ha, Andrew Carson, Univ. of Pittsburgh Medical Ctr. (USA); Kang Kim, Univ. of Pittsburgh Medical Ctr. (USA) and Univ. of Pittsburgh (USA) . . . . . [8223-93]

Photoacoustic tomography of the monkey brain using virtual point detectors: theory, Chao Huang, Robert W. Schoonover, Liming Nie, Zijian Guo, Lihong V. Wang, Mark A. Anastasio, Washington Univ. in St. Louis (USA) . . . . . [8223-94]

Compensation of shear waves in photoacoustic tomography with layered acoustic media, Robert W. Schoonover, Mark A. Anastasio, Washington Univ. in St. Louis (USA) . . . . . [8223-95]

Ultrasound-modulated optical tomography using slow light in spectral-hole burning materials, Huiliang Zhang, Harvard Univ. (USA); Mahmood Sabooni, Lars Rippe, Stefan Kröll, Lund Univ. (Sweden); Lihong V. Wang, Washington Univ. in St. Louis (USA); Philip R. Hemmer, Texas A&M Univ. (USA) . . . [8223-96]

Conference 8223 · Room: 305 (Esplanade)

Imaging the ultrasound field and shear-wave propagation using acousto-optic laser speckle contrast analysis (AO-LASCA), Lipei Song, Yi Cheng, Rui Li, Mengxing Tang, Daniel S. Elson, Imperial College London (United Kingdom) . . . . . [8223-97]

Passive acoustic radiometer for non-invasive monitoring of internal temperature during local laser hyperthermia, Pavel V. Subochev, Institute of Applied Physics (Russian Federation); Marina A. Sirotkina, Nizhny Novgorod State Medical Academy (Russian Federation); Vladimir V. Klin'shov, Anatoly D. Mansfel'd, Institute of Applied Physics (Russian Federation) . . . . . [8223-98]

Conjugate gradient preconditioning methods with symmetric algebraic reconstruction technique in photoacoustic imaging, Xueyan Liu, Northeastern Univ. (China); Jie Tian, Dong Han, Guodong Li, Institute of Automation (China); Wei Guo, Beijing Univ. of Technology (China); Chenghu Qin, Xibo Ma, Xin Yang, Institute of Automation (China) . . . . . [8223-99]

Ultrafast ultrasound and photoacoustic co-registered imaging system based on FPGA parallel processing, Umar S. Alqasemi, Hai Li, Andres Aguirre, Quing Zhu, Univ. of Connecticut (USA) . . . . . [8223-100]

DVD pickup head based optical resolution photoacoustic microscopy, Po-Hsun Wang, Meng-Lin Li, National Tsing Hua Univ. (Taiwan) . . . . . [8223-101]

Influence of laser pulse width to the photoacoustic temporal waveform and the image resolution with a solid state excitation laser, Kaku Irisawa, Kazuhiro Hirota, Kazuhiro Tsujita, FUJIFILM Corp. (Japan); Takeshi Hirasawa, Miya Ishihara, National Defense Medical College (Japan) . . . . . [8223-102]

New adaptive beamforming with spatially smoothed coherence factor for photoacoustic imaging, Jeeun Kang, Jin Ho Chang, Yangmo Yoo, Tai-Kyong Song, Sogang Univ. (Korea, Republic of) . . . . . [8223-103]

Model-based image enhancement in optoacoustic tomography of the mouse brain, Amir Rosenthal, Thomas Jetzfellner, Xosé Luís Deán Ben, Daniel Razansky, Vasilis Ntziachristos, Helmholtz Zentrum München GmbH (Germany) . . . . . [8223-104]

An algorithm for sensing venous oxygenation using ultrasound-modulated light enhanced by microbubbles, Jack E. P. Honeysett, Eleanor Stride, Terence S. Leung, Univ. College London (United Kingdom) . . . . . [8223-105]

Real-time imaging of renal clearance using multispectral optoacoustic tomography, Stefan Morscher, Neal C. Burton, Adrian Taruttis, Nikolaos C. Deliolanis, Daniel Razansky, Vasilis Ntziachristos, Helmholtz Zentrum München GmbH (Germany) and Technische Univ. München (Germany) . . . . . [8223-106]

Elasticity characterisation in turbid tissue mimicking phantoms by optical tracking of shear waves, Yi Cheng, Rui Li, Daniel S. Elson, Mengxing Tang, Imperial College London (United Kingdom) . . . . . [8223-107]

On laser-induced ultrasound generated in a thin semi-transparent layered polymer structure, Erika T. Svanström, Torbjörn Löfqvist, Jerker Delsing, Luleå Univ. of Technology (Sweden) . . . . . [8223-108]

Continuous wavelet-transform analysis of photoacoustic signal waveform to determine optical absorption coefficient, Takeshi Hirasawa, Miya Ishihara, National Defense Medical College (Japan); Kazuhiro Tsujita, Kazuhiro Hirota, Kaku Irisawa, FUJIFILM Corp. (Japan); Manabu Kitagaki M.D., Masanori Fujita M.D., Makoto Kikuchi, National Defense Medical College (Japan) . . . . [8223-109]

Functional photoacoustic micro-imaging of rat cerebral hemodynamic response function in single vessels during forepaw electrical stimulation, Lun-De Liao, National Chiao Tung Univ. (Taiwan); You-Yin Chen, National Yang Ming Univ. (Taiwan); Chin-Teng Lin, Jyh-Yeong Chang, National Chiao Tung Univ. (Taiwan); Meng-Lin Li, National Tsing Hua Univ. (Taiwan) . . . . . [8223-110]

Photoacoustic array imaging of calcifications: phantom study, Yao-You Cheng, Tsai-Chu Hsiao, National Tsing Hua Univ. (Taiwan); Wan-Ting Tien, Shih-Bin Luo, De-Yi Chiou, Industrial Technology Research Institute (Taiwan); Meng-Lin Li, National Tsing Hua Univ. (Taiwan) . . . . . [8223-111]

Signal recovered from a photoacoustic imaging based on a long-focal-zone transducer, Wenming Xie, Zhiping Zeng, Li Li, Zhifang Li, Hui Li, Fujian Normal Univ. (China) . . . . . [8223-112]

Single-mode polymer fiber line detector for photoacoustic tomography, Hubert Grün, Thomas Berer, Karoline Felbermayer, RECENDT GmbH (Austria); Günther Paltauf, Karl-Franzens-Univ. Graz (Austria); Peter Burgholzer, RECENDT GmbH (Austria) . . . . . [8223-113]

Optical detection of photoacoustic waves using phase sensitive low-coherence interferometry, Boris Hermann, Michelle Gabriele Sandrian, Boris Pova?ay, Bernd Hofer, Wolfgang Drexler, Medizinische Univ. Wien (Austria) . . . . . [8223-114]

Ultrasound-guided photoacoustic image reconstruction, Pieter Kruizinga, Frits Mastik, Erasmus MC (Netherlands); Nico de Jong, Antonius F. W. van der Steen, Erasmus MC (Netherlands) and Interuniversity Cardiology Institute of The Netherlands (Netherlands); Gijs van Soest, Erasmus MC (Netherlands) . . . . . [8223-115]

Photoacoustic imaging of the near-infrared fluorescent protein iRFP in vivo, Arie Krumholz, Washington Univ. in St. Louis (USA); Grigory S. Filonov, Albert Einstein College of Medicine (USA); Jun Xia, Junjie Yao, Washington Univ. in St. Louis (USA); Vladislav V. Verkhusha, Albert Einstein College of Medicine (USA); Lihong V. Wang, Washington Univ. in St. Louis (USA) . . . . . [8223-116]

Image quality assessment using different types of optical diffusers for photoacoustic tomography, Do-Hyun Kim, U.S. Food and Drug Administration (USA); Sanghun Ryu, Dong-Ho Shin, Chul-Gyu Song, Chonbuk National Univ. (Korea, Republic of) . . . . . [8223-155]

Monday 23 January

SESSION 5

Room: 305 (Esplanade) . . . . . Mon. 8:00 to 9:45 am

Microscopy

Session Chairs: **Lihong V. Wang,** Washington Univ. in St. Louis (USA); **Qifa Zhou,** The Univ. of Southern California (USA)

8:00 am: **3D high-resolution pure optical photoacoustic microscopy**, Zhixing Xie, Univ. of Michigan Medical School (USA); Sung-Liang Chen, Tao Ling, L. Jay Guo, Univ. of Michigan (USA); Paul L. Carson, Xueding Wang, Univ. of Michigan Medical School (USA) . . . . . [8223-30]

8:15 am: **In vivo imaging of larvae by photoacoustic microscopy**, Shuoqi Ye, Ran Yang, Jingwei Xiong, Peking Univ. (China); K. Kirk Shung, Qifa Zhou, Univ. of Southern California (USA); Changhui Li, Peking Univ. (China); Qiushi Ren, Peking Univ. (China) and Shanghai JiaoTong Univ. (China) . . . . . [8223-31]

8:30 am: **Imaging dynamic processes using fiber laser optical-resolution photoacoustic microscopy**, Wei Shi, Parsin Hajireza, Alexander Forbrich, Roger J. Zemp, Univ. of Alberta (Canada) . . . . . [8223-32]

8:45 am: **Optoacoustic microscopy system based on an off-axis parabolic reflector**, Dmitri Tsyboulski, André Conjusteau, Alexander A. Oraevsky, TomoWave Labs., Inc. (USA) . . . . . [8223-33]

9:00 am: **Multiparameter photoacoustic microscopy of tumor micro-environment**, Song Hu, Washington Univ. in St. Louis (USA); Rebecca Sohn, Zhi-Hong Lu, Washington Univ. School of Medicine in St. Louis (USA); Brian T. Soetikno, Qiaonan Zhong, Junjie Yao, Konstantin I. Maslov, Washington Univ. in St. Louis (USA); Jeffrey M. Arbeit, Washington Univ. School of Medicine in St. Louis (USA); Lihong V. Wang, Washington Univ. in St. Louis (USA) . . . . [8223-34]

9:15 am: **Mosaicing for fast wide-field-of-view optical-resolution photoacoustic microscopy**, Peng Shao, Ryan Chee, Alexander Forbrich, Roger J. Zemp, Univ. of Alberta (Canada) . . . . . [8223-35]

9:30 am: **A fast multiwavelength-scanning photoacoustic microscope based on a digital mirror device**, Yu Wang, Konstantin I. Maslov, Lihong V. Wang, Washington Univ. in St. Louis (USA) . . . . . [8223-36]

Coffee Break . . . . . 9:45 to 10:15 am

SESSION 6

Room: 305 (Esplanade) . . . . . Mon. 10:15 am to 12:00 pm

Dual Modality Imaging and Monitoring

Session Chairs: **Martin Frenz,** Univ. Bern (Switzerland); **Stanislav Y. Emelianov,** The Univ. of Texas at Austin (USA)

10:15 am: **Optoacoustic temperature monitoring during HIFU impact on biological tissues: ex-vivo study and numerical simulation of 2D temperature reconstruction**, Ivan M. Pelivanov, Sergey M. Nikitin, Lomonosov Moscow State Univ. (Russian Federation); Tatiana Khokhlova, Univ. of Washington (USA) . . . . . [8223-37]

10:30 am: **Combined optoacoustic and high-frequency ultrasound imaging of live mouse embryos**, Parag V. Chitnis, Riverside Research Institute (USA); Orlando Aristizábal, New York Univ. School of Medicine (USA); Erwan Filoux, Ashwinkumar Sampathkumar, Jonathan Mamou, Riverside Research Institute (USA); Daniel H. Turnbull, New York Univ. School of Medicine (USA); Jeffrey A. Ketterling, Riverside Research Institute (USA) . . . . . [8223-38]

10:45 am: **In vivo combined photoacoustic and Doppler ultrasound imaging**, Yan Jiang, Tyler Harrison, Alexander Forbrich, Roger J. Zemp, Univ. of Alberta (Canada) . . . . . [8223-39]

11:00 am: **Functional dual-modality photoacoustic and ultrasonic endoscopy in vivo**, Joon-Mo Yang, Christopher P. Favazza, Washington Univ. in St. Louis (USA); Ruimin Chen, The Univ. of Southern California (USA); Junjie Yao, Xin Cai, Konstantin I. Maslov, Washington Univ. in St. Louis (USA); Qifa Zhou, K. Kirk Shung, The Univ. of Southern California (USA); Lihong V. Wang, Washington Univ. in St. Louis (USA) . . . . . [8223-40]

11:15 am: **Optoacoustic generation of high-amplitude focused ultrasound by using carbon-nanotube polymer composite films**, Hyoung Won Baac, Adam Maxwell, Jong G. Ok, Kuang-Wei Lin, Zhen Xu, L. Jay Guo, Univ. of Michigan (USA) . . . . . [8223-41]

11:30 am: **Combined optical-resolution photoacoustic and fluorescence micro-endoscopy**, Peng Shao, Parsin Hajireza, Wei Shi, Roger J. Zemp, Univ. of Alberta (Canada) . . . . . [8223-42]

11:45 am: **Real-time intravascular ultrasound/photoacoustic imaging system with omni-directional light excitation**, Bao-Yu Hsieh, Pai-Chi Li, National Taiwan Univ. (Taiwan) . . . . . [8223-43]

Lunch Break . . . . . 12:00 to 1:30 pm

SESSION 7

Room: 305 (Esplanade) . . . . . Mon. 1:30 to 5:45 pm

New Methods and Novel Techniques

Session Chairs: **A. Claude Boccara,** Ecole Supérieure de Physique et de Chimie Industrielles (France); **Charles A. DiMarzio,** Northeastern Univ. (USA)

1:30 pm: **New photoacoustic cell with diamond window cover for mid-infrared investigations on biological samples**, Jonas Kottmann, Julien M. Rey, Markus W. Sigrist, ETH Zurich (Switzerland) . . . . . [8223-44]

1:45 pm: **Time-reversed ultrasonically encoded (TRUE) optical focusing in reflection mode: demonstrations in tissue mimicking phantoms and ex vivo tissue**, Puxiang Lai, Xiao Xu, Honglin Liu, Yuta Suzuki, Lihong V. Wang, Washington Univ. in St. Louis (USA) . . . . . [8223-45]

2:00 pm: **Non-contact photoacoustic tomography and ultrasonography for biomedical imaging**, Guy Rousseau, Daniel Lévesque, Alain Blouin, Jean-Pierre Monchalin, National Research Council Canada (Canada) . . . . . [8223-46]

2:15 pm: **Flow-dependant photothermal modulation of the photoacoustic response**, Adi Sheinfeld, Avishay Eyal, Tel Aviv Univ. (Israel) . . . . . [8223-47]

2:30 pm: **Multispectral photoacoustic coded excitation using pseudorandom codes**, Martin F. Beckmann, Claus-Stefan Friedrich, Martin P. Mienkina, Nils C. Gerhardt, Martin R. Hofmann, Georg Schmitz, Ruhr-Univ. Bochum (Germany) . . . . . [8223-48]

2:45 pm: **Acoustic reflector combined with optical detection for photoacoustic section imaging**, Robert Nuster, Sibylle Gratt, Klaus Passler, Guenther Paltauf, Karl-Franzens-Univ. Graz (Austria) . . . . . [8223-49]

Coffee Break . . . . . 3:00 to 3:30 pm

3:30 pm: **Contactless photoacoustic imaging of biological samples**, Thomas Berer, Armin Hochreiner, Hubert Grün, Peter Burgholzer, RECENDT GmbH (Austria) . . . . . [8223-50]

3:45 pm: **Miniature fiber optic photoacoustic imaging probes for micro-endoscopic applications**, Edward Z. Zhang, Paul Beard, Univ. College London (United Kingdom) . . . . . [8223-51]

4:00 pm: **Vibrational photoacoustic microscopy for deep tissue bond-selective imaging**, Ji-Xin Cheng, Purdue Univ. (USA) . . . . . [8223-52]

4:15 pm: **Frequency domain photoacoustic correlation imaging: novel methodology for non-invasive imaging of biological tissues**, Sergey A. Telenkov, Rudolf Alwi, Univ. of Toronto (Canada); Willa Shi, Emily Chen, Alex I. Vitkin, Ontario Cancer Institute (Canada); Andreas Mandelis, Univ. of Toronto (Canada) . . . . . [8223-142]

4:30 pm: **Real-time photoacoustic imaging with optical ultrasound detection**, Robert Nuster, Guenther Paltauf, Karl-Franzens-Univ. Graz (Austria) . . . . . [8223-54]

4:45 pm: **Novel optoacoustic system for noninvasive, continuous monitoring of cerebral venous blood oxygenation**, Yuriy Y. Petrov, Irene Y. Petrov, Donald S. Prough, Rinat O. Esenaliev, The Univ. of Texas Medical Branch (USA) . . . . . [8223-55]

5:00 pm: **Noninvasive, optoacoustic monitoring of cerebral venous blood oxygenation in newborns**, Irene Y. Petrov, Karon E. Wynne, Yuriy Y. Petrov, Rinat O. Esenaliev, C. Joan Richardson, Donald S. Prough, The Univ. of Texas Medical Branch (USA) . . . . . [8223-56]

5:15 pm: **Impulse-based near-field thermoacoustic tomography of small animals**, Stephan Kellnberger, Daniel Razansky, Vasilis Ntziachristos, Helmholtz Zentrum München GmbH (Germany) . . . . . [8223-57]

5:30 pm: **Near-field radio-frequency thermo-acoustic imaging based on transmission lines for optimized performance,** Murad Omar, Stephan Kellnberger, Technische Univ. München (Germany) and Helmholtz Zentrum München GmbH (Germany); George Sergiadis, Aristotle Univ. of Thessaloniki (Greece); Daniel Razansky, Vasilis Ntziachristos, Technische Univ. München (Germany) and Helmholtz Zentrum München GmbH (Germany) . . . . . [8223-58

POSTERS - MONDAY

Room: 103 (Exhibit Level) . . . . . Mon. 5:30 to 7:30 pm

Conference attendees are invited to attend the BiOS poster session on Monday evening. Come view the posters, enjoy light refreshments, ask questions, and network with colleagues in your field. Authors of poster papers will be present to answer questions concerning their papers. Attendees are required to wear their conference registration badges to the poster sessions. Poster authors, view poster presentation guidelines and set-up instructions at http://spie.org/x27476.xml.

Photoacoustic and ultrasonic image co-registration using a phased array probe and frequency domain correlation processing, Sergey A. Telenkov, Rudolf Alwi, Univ. of Toronto (Canada); Willa Shi, Emily Chen, Alex I. Vitkin, Ontario Cancer Institute (Canada); Andreas Mandelis, Univ. of Toronto (Canada) . . . . . [8223-53]

Photoacoustic tomography of breast phantoms based on a custom-made linear array transducer, Wenfeng Xia, Daniele Piras, Johan Van Hespen, Wiendelt Steenbergen, Ton G. van Leeuwen, Srirang Manohar, Univ. Twente (Netherlands) . . . . . [8223-117]

Detection and characterization of red blood cell (RBC) aggregation with photoacoustics, Eno Hysi, Ratan K. Saha, Min Rui, Michael C. Kolios, Ryerson Univ. (Canada) . . . . . [8223-118]

Optimising the excitation and detection parameters for deep-tissue photoacoustic imaging applications, Thomas J. Allen, Edward Zhang, Paul Beard, Univ. College London (United Kingdom) . . . . . [8223-119]

3D photoacoustic imaging via staring, sparse approach at 0.7 FPS, Michael B. Roumeliotis, Jeffrey J. L. Carson, Lawson Health Research Institute (Canada) . . . . . [8223-120]

Laser-diode based 10MHz photoacoustic Doppler flowmetry at 830 nm, Adi Sheinfeld, Avishay Eyal, Tel-Aviv Univ. (Israel) . . . . . [8223-121]

Wide-spectral range quantitative photoacoustic spectroscopy to measure non-linear optical absorption of hemoglobin, Amos Danielli, Konstantin I. Maslov, Lihong V. Wang, Washington Univ. in St. Louis (USA) . . . . . [8223-122]

Monitoring of streptozotocin-induced diabetes in a mouse model by photoacoustic microscopy, Arie Krumholz, Junjie Yao, Lihong V. Wang, Washington Univ. in St. Louis (USA) . . . . . [8223-123]

Image quality improvement for photoacoustic imaging systems employing linear transducer arrays, Adam Petschke, Patrick J. La Rivière, The Univ. of Chicago Medical Ctr. (USA) . . . . . [8223-124]

Photoacoustic imaging of RF ablations in cardiac tissue, Richard R. Bouchard, The Univ. of Texas M.D. Anderson Cancer Ctr. (USA); Luigi Di Base, Andrea Natale, St. David's Medical Ctr. (USA); Stanislav Y. Emelianov, The Univ. of Texas at Austin (USA) and The Univ. of Texas M.D. Anderson Cancer Ctr. (USA) . . . . . [8223-125]

Photoacoustic microscopy imaging of spheroids with endogenous and exogenous contrast, Min Rui, Michael C. Kolios, Ryerson Univ. (Canada) . . . . . [8223-126]

2.5-mm outer diameter photoacoustic endoscopic mini-probe based on highly sensitive PMN-PT ultrasonic transducer, Joon-Mo Yang, Washington Univ. in St. Louis (USA); Ruimin Chen, The Univ. of Southern California (USA); Christopher P. Favazza, Junjie Yao, Washington Univ. in St. Louis (USA); Qifa Zhou, K. Kirk Shung, The Univ. of Southern California (USA); Lihong V. Wang, Washington Univ. in St. Louis (USA) . . . . . [8223-127]

A hand-held, low-cost photoacoustic microscopic probe, Bin Huang, Konstantin I. Maslov, William D. Richard, Lihong V. Wang, David M. Zar, Washington Univ. in St. Louis (USA) . . . . . [8223-128]

Tissue-mimicking phantoms for photoacoustic and ultrasonic imaging, Richard R. Bouchard, The Univ. of Texas M.D. Anderson Cancer Ctr. (USA); Jason Cook, The Univ. of Texas at Austin (USA); Stanislav Y. Emelianov, The Univ. of Texas at Austin (USA) and M.D. Anderson Cancer Ctr. (USA). [8223-129]

Conference 8223 · Room: 305 (Esplanade)

In vivo quantitative evaluation of gold nanocages' kinetics in sentinel lymph nodes by photoacoustic imaging, Xin Cai, Weiyang Li, Washington Univ. in St. Louis (USA); Chulhong Kim, Univ. at Buffalo (USA); Yuchen Yuan, Younan Xia, Lihong V. Wang, Washington Univ. in St. Louis (USA) . . . . . [8223-130]

Multiphoton photoacoustic microscopic imaging of fluorescently labeled neuron populations, Gali Sela, Hod Dana, Inbar Brosh, Technion-Israel Institute of Technology (Israel); Daniel Razansky, Helmholtz Zentrum München GmbH (Germany); Shy Shoham, Technion-Israel Institute of Technology (Israel) . . . . . [8223-131]

Design of an optimum ultrasound pattern to minimize multiple-scattered light reflected from inhomogeneous tissue, Pedro Pereira, Sherif S. Sherif, Univ. of Manitoba (Canada) . . . . . [8223-132]

Modeling comparison of optical-resolution photoacoustic microscopy and optical coherence tomography, Yan Liu, Chi Zhang, Song Hu, Yuta Suzuki, Zhun Xu, Silvina L. Ferradal, Lihong V. Wang, Washington Univ. in St. Louis (USA) . . . . . [8223-133]

Dichroic photoacoustic microscopy of amyloid plaques in a transgenic mouse model, Konstantin I. Maslov, Song Hu, Ping Yan, Jin-Moo Lee, Lihong V. Wang, Washington Univ. in St. Louis (USA) . . . . . [8223-134]

Time-resolved transient absorption ultrasonic microscopy measurements of the ground state recovery time, Ryan L. Shelton, Brian E. Applegate, Texas A&M Univ. (USA) . . . . . [8223-135]

Photoacoustic microscopy of intestinal hemodynamics following massive small bowel resection, Junjie Yao, Washington Univ. in St. Louis (USA); Kathryn J. Rowland, Washington Univ. School of Medicine in St. Louis (USA); Lidai Wang, Konstantin I. Maslov, Washington Univ. in St. Louis (USA); Brad W. Warner, Washington Univ. School of Medicine in St. Louis (USA); Lihong V. Wang, Washington Univ. in St. Louis (USA) . . . . . [8223-136]

Molecular probes for imaging of enzyme activity by photoacoustic lifetime imaging (PALI), Ekaterina Morgounova, Qi Shao, Sajeda Abdo, Mickael Wilson, George Barany, Shai Ashkenazi, Univ. of Minnesota, Twin Cities (USA) . . . . . [8223-137]

Modeling optical phase conjugation of ultrasonically encoded signal utilizing finite-difference time-domain simulations, Joseph L. Hollmann, Charles A. DiMarzio, Northeastern Univ. (USA) . . . . . [8223-138]

Inducible expression of photoacoustic reporter gene tyrosinase in cells using a single plasmid, Robert J. Paproski, Roger J. Zemp, Univ. of Alberta (Canada) . . . . . [8223-139]

Characterization of dual-contrast microbubbles for photoacoustic and ultrasound imaging, Robin F. Castelino, Univ. of Toronto (Canada) and Sunnybrook Health Sciences Ctr. (Canada); Amanda L. Martin, Sunnybrook Health Sciences Ctr. (Canada); F. Stuart Foster, Univ. of Toronto (Canada) and Sunnybrook Health Sciences Ctr. (Canada) . . . . . [8223-140]

Signal-to-noise-ratio scaled coherence weighting for photoacoustic array imaging, Yu-Hsin Wang, Pai-Chi Li, National Taiwan Univ. (Taiwan) . . [8223-141]

Optoacoustic signal characterization of laser heated tissues, Annie Ladéroute, Univ. of Prince Edward Island (Canada); Michelle P. Patterson, Univ. of Prince Edward Island (Canada) and Atlantic Veterinary College (Canada); Michael C. Kolios, Ryerson Univ. (Canada); William M. Whelan, Univ. of Prince Edward Island (Canada) and Atlantic Veterinary College (Canada) . . . [8223-143]

Measuring metabolic rate of oxygen with combined photoacoustic microscopy and optical coherent tomography in small animals, Tan Liu, Northwestern Univ. (USA); Shuliang Jiao, The Univ. of Southern California (USA); Hao F. Zhang, Northwestern Univ. (USA) . . . . . [8223-144]

High-sensitivity polymer inverted-rib optical waveguide interferometric sensor for optoacoustic imaging, Daniel C. Gallego, Horacio Lamela, Univ. Carlos III de Madrid (Spain); Meng Wang, Univ. of Oulu (Finland); Jussi Hiltunen, VTT Technical Research Ctr. of Finland (Finland); Risto Myllylä, Univ. of Oulu (Finland) . . . . . [8223-145]

PEG-coated gold nanorods conjugated with monoclonal antibodies for preclinical research in optoacoustic imaging and sensing, Anton Liopo, André Conjusteau, Alexander A. Oraevsky, TomoWave Labs., Inc. (USA) . . . . . [8223-146]

Vessel segmentation analysis of ischemic stroke images acquired with photoacoustic microscopy, Brian T. Soetikno, Song Hu, Washington Univ. in St. Louis (USA); Ernie Gonzales, Washington Univ. School of Medicine in St. Louis (USA); Qiaonan Zhong, Konstantin I. Maslov, Washington Univ. in St. Louis (USA); Jin-Moo Lee, Washington Univ. School of Medicine in St. Louis (USA); Lihong V. Wang, Washington Univ. in St. Louis (USA) . . . . . [8223-147]

Numerical simulation based photoacoustic design parameter optimization for deep tissue imaging, Zhaohui Wang, Seung-Han Ha, Univ. of Pittsburgh Medical Ctr. (USA); Kang Kim, Univ. of Pittsburgh Medical Ctr. (USA) and Univ. of Pittsburgh (USA) . . . . . [8223-148]

Application of laser pulse stretching scheme for efficiently delivering laser energy in photoacoustic imaging, Tianheng Wang, Patrick D. Kumavor, Quing Zhu, Univ. of Connecticut (USA) . . . . . [8223-149]

Photoacoustic imaging using Porphyrin derivatives as exogeneous contrast agents, Akram Abuteen, Saeid Zanganeh, Joshua Akhigbe, Nrusingh C. Biswal, Andres Aguirre, Christian Brückner, Quing Zhu, Univ. of Connecticut (USA) . . . . . [8223-150]

Investigation of a quantitative photoacoustic tomography fitting procedure on multiple targets in reflection geometry with diffuse optical measurement assistance, Chen Xu, Patrick D. Kumavor, Quing Zhu, Univ. of Connecticut (USA) . . . . . [8223-151]

Optoacoustic monitoring of cerebral venous blood oxygenation in rats with traumatic brain injury, Karon E. Wynne, Douglas S. Dewitt, Yuriy Y. Petrov, Irene Y. Petrov, Margaret A. Parsley, Rinat O. Esenaliev, Donald S. Prough, The Univ. of Texas Medical Branch (USA) . . . . . [8223-152]

Integrated scanning confocal photothermal-lens and photoacoustic microscopy, Dmitry A. Nedosekin, Ekaterina I. Galanzha, Robert J. S. Reis, Vladimir P. Zharov, Univ. of Arkansas for Medical Sciences (USA) . . . [8223-153]

Quantification of optical absorption coefficient from acoustic spectra in the optical diffusive regime using photoacoustic microscopy, Zijian Guo, Christopher P. Favazza, Lihong V. Wang, Washington Univ. in St. Louis (USA) . . . . . [8223-154]

Tuesday 24 January

SESSION 8

Room: 305 (Esplanade) . . . . . Tues. 8:00 to 9:15 am

Imaging Nanoparticles and Contrast Agents

Session Chairs: **Pai-Chi Li,** National Taiwan Univ. (Taiwan); **Matthew O'Donnell,** Univ. of Washington (USA)

8:00 am: **Ultrasound guided spectroscopic photoacoustic imaging for in vivo monitoring of mesenchymal stem cells labeled with nanotracers**, Seung Yun Nam, Laura M. Ricles, Laura J. Suggs, Stanislav Y. Emelianov, The Univ. of Texas at Austin (USA) . . . . . [8223-59]

8:15 am: **Intravascular photoacoustic imaging of gold nanorod-labeled atherosclerotic plaques**, Douglas E. Yeager, Bo Wang, Andrei B. Karpiouk, The Univ. of Texas at Austin (USA); James H. Amirian, The Univ. of Texas Health Science Ctr. at Houston (USA); Konstantin Sokolov, The Univ. of Texas M.D. Anderson Cancer Ctr. (USA) and The Univ. of Texas at Austin (USA); Stanislav Y. Emelianov, The Univ. of Texas at Austin (USA) and The Univ. of Texas M.D. Anderson Cancer Ctr. (USA) . . . . . [8223-60]

8:30 am: **Trapping and dynamic manipulation with magnetomotive photoacoustic imaging of targeted microspheres mimicking metastatic cancer cells trafficking in the vasculature**, Chen-Wei Wei, Jinjun Xia, Univ. of Washington (USA); Ivan M. Pelivanov, Univ. of Washington (Russian Federation); Xiaoge Hu, Xiaohu Gao, Matthew O'Donnell, Univ. of Washington (USA) . . . . . [8223-61]

8:45 am: **Dual-contrast photoacoustic nanodroplets: in vivo imaging results**, Katheryne E. Wilson, Alexander Hannah, Kimberly Homan, Stanislav Y. Emelianov, The Univ. of Texas at Austin (USA) . . . . . [8223-62]

9:00 am: **In vivo photoacoustic flow cytometry in plants: direct study of nanomaterials uptake and accumulation**, Dmitry A. Nedosekin, Univ. of Arkansas for Medical Sciences (USA); Mariya V. Khodakovskaya, Alexandru S. Biris, Univ. of Arkansas at Little Rock (USA); Ekaterina I. Galanzha, Vladimir P. Zharov, Univ. of Arkansas for Medical Sciences (USA) . . . . . [8223-63]

BiOS

SESSION 9

Room: 305 (Esplanade) . . . . . Tues. 9:15 to 10:15 am

Imaging and Sensing at Cellular Level

Session Chairs: **Steven L. Jacques,** Oregon Health & Science Univ. (USA); **Vladimir P. Zharov,** Univ. of Arkansas for Medical Sciences (USA)

9:15 am: **Photoacoustic cystography**, Chulhong Kim, Mansik Jeon, Univ. at Buffalo (USA); Lihong V. Wang, Washington Univ. in St. Louis (USA) . . [8223-64]

9:30 am: **Photoacoustic imaging of oxygen release from hemoglobin in single red blood cells in vivo**, Lidai Wang, Lihong V. Wang, Washington Univ. School of Medicine in St. Louis (USA). . . . . [8223-65]

9:45 am: **Label-free photoacoustic microscopy of cytochrome C in mitochondria**, Chi Zhang, Konstantin I. Maslov, Lihong V. Wang, Washington Univ. in St. Louis (USA) . . . . . [8223-66]

10:00 am: **In vivo imaging of cell nuclei by photoacoustic microscopy without staining**, Da-Kang Yao, Washington Univ. in St. Louis (USA); Ruimin Chen, The Univ. of Southern California (USA); Konstantin I. Maslov, Washington Univ. in St. Louis (USA); Qifa Zhou, The Univ. of Southern California (USA); Lihong V. Wang, Washington Univ. in St. Louis (USA) . . . . . [8223-67]

Coffee Break . . . . . 10:15 to 10:45 am

SESSION 10

Room: 305 (Esplanade) . . . . . Tues. 10:45 am to 12:00 pm

Signal and Image Processing

Session Chairs: **Mark A. Anastasio,** Washington Univ. in St. Louis (USA); **Andreas Mandelis,** Univ. of Toronto (Canada)

10:45 am: **Application of iterative image reconstruction algorithms to three-dimensional optoacoustic tomography**, Kun Wang, Washington Univ. in St. Louis (USA); Alexander A. Oraevsky, TomoWave Labs., Inc. (USA); Mark A. Anastasio, Washington Univ. in St. Louis (USA) . . . . . [8223-68]

11:00 am: **Adapted directivity approach for photoacoustic imaging reconstruction**, Daniele Piras, Wenfeng Xia, Michelle Heijblom, Wiendelt Steenbergen, Univ. Twente (Netherlands); Ton G. van Leeuwen, Univ. Amsterdam (Netherlands) and Univ. Twente (Netherlands); Srirang Manohar, Univ. Twente (Netherlands) . . . . . [8223-69]

11:15 am: **Analysis of the role of shear waves in transcranial photoacoustic tomography**, Robert W. Schoonover, Lihong V. Wang, Mark A. Anastasio, Washington Univ. in St. Louis (USA) . . . . . [8223-70]

11:30 am: **Spatial resolution and sensitivity in photoacoustic tomography taking noise into account: from point-like detectors to large integrating detectors**, Peter Burgholzer, RECENDT GmbH (Austria); Thomas Berer, RECENDT GmbH (Germany); Hubert Grün, RECENDT GmbH (Austria); Robert Nuster, Günther Paltauf, Karl-Franzens-Univ. Graz (Austria) . . . . . [8223-71]

11:45 am: **Sparsity regularized data-space restoration in optoacoustic tomography**, Kun Wang, Washington Univ. in St. Louis (USA); Alexander A. Oraevsky, TomoWave Labs., Inc. (USA); Mark A. Anastasio, Washington Univ. in St. Louis (USA) . . . . . [8223-72]

Lunch Break . . . . . 12:00 to 1:30 pm

SESSION 11

Room: 305 (Esplanade) . . . . . Tues. 1:30 to 3:00 pm

Ultrasound Modulated Optical Tomography I

Joint Session with Conference 8272

Session Chairs: **Lihong V. Wang,** Washington Univ. in St. Louis (USA); **Philip R. Hemmer,** Texas A&M Univ. (USA)

1:30 pm: **Signals, noises, and detection schemes in ultrasonically modulated optical imaging** *(Invited Paper)*, François Ramaz, Ecole Supérieure de Physique et de Chimie Industrielles (France); Michel Gross, Univ. Montpellier 2 (France); A. Claude Boccara, Ecole Supérieure de Physique et de Chimie Industrielles (France) . . . . . [8223-73]

1:45 pm: **Ultrasound-modulated optical tomography of biological tissue using spectral-hole burning** *(Invited Paper)*, Xiao Xu, Honglin Liu, Washington Univ. in St. Louis (USA); Sri-Rajasekhar Kothapalli, Stanford Univ. (USA); Puxiang Lai, Yuta Suzuki, Lihong V. Wang, Washington Univ. in St. Louis (USA) . . . . . [8223-74]

2:00 pm: **Creating filters for shot-noise-limited Ultrasound Optical Tomography (UOT)** *(Invited Paper)*, Mahmood Sabooni, Lund Univ. (Sweden); Huiliang Zhang, Texas A&M Univ. (USA); Lars Rippe, Lund Univ. (Sweden); Chulhong Kim, Washington Univ. in St. Louis (USA); Stefan Kroll, Lund Univ. (Sweden); Philip Hemmer, Texas A&M Univ. (USA) . . . . . [8272-12]

2:15 pm: **Rare-earth-doped materials with application to optical signal processing, quantum information science, and medical imaging technology** *(Invited Paper)*, Rufus L. Cone, Charles W. Thiel, Montana State Univ. (USA); Yongchen Sun, The Univ. of South Dakota (USA); Thomas Böttger, Univ. of California, San Francisco (USA); Roger M. Macfarlane, Montana State Univ. (USA) . . . . . [8272-13]

2:30 pm: **Recent progress in ultrasound-mediated fluorescence** *(Invited Paper)*, Baohong Yuan, Yuan Liu, The Univ. of Texas at Arlington (USA) . . . . . [8223-75]

2:45 pm: **The potential of ultrasound-modulated optical sensing in clinical monitoring** *(Invited Paper)*, Terence S. Leung, Univ. College London (United Kingdom) . . . . . [8223-76]

Coffee Break . . . . . 3:00 to 3:30 pm

SESSION 12

Room: 305 (Esplanade) . . . . . Tues. 3:30 to 5:30 pm

Ultrasound Modulated Optical Tomography II

Joint Session with Conference 8272

Session Chairs: **Lihong V. Wang,** Washington Univ. in St. Louis (USA); **Philip R. Hemmer,** Texas A&M Univ. (USA)

3:30 pm: **Atom like centers in solids for nanophotonic and quantum devices**, Zameer U. Hasan, Temple Univ. (USA) . . . . . [8272-14]

3:45 pm: **Acoustic radiation force assisted ultrasound modulated optical tomography** *(Invited Paper)*, Mengxing Tang, Rui Li, Yi Cheng, Christopher W. Dunsby, Robert J. Eckersley, Daniel S. Elson, Imperial College London (United Kingdom) . . . . . [8223-77]

4:00 pm: **Improving signal-to-noise ratio and spatial resolution in ultrasound modulated optical tomography** *(Invited Paper)*, Stephen P. Morgan, Haowen Ruan, Nam Trung Huynh, Melissa L. Mather, Diwei He, John Crowe, Felicity R. Rose, Barrie R. Hayes-Gill, The Univ. of Nottingham (United Kingdom) . . . . . [8223-78]

4:15 pm: **Spectral-hole burning techniques for ultrasound-modulated optical tomography** *(Invited Paper)*, Huiliang Zhang, Texas A&M Univ. (USA); Mahmood Sabooni, Lars Rippe, Lund Univ. (Sweden); Chulhong Kim, Washington Univ. in St. Louis (USA); Stefan Kroll, Lund Univ. (Sweden); Lihong V. Wang, Washington Univ. in St. Louis (USA); Philip R. Hemmer, Texas A&M Univ. (USA) . . . . . [8272-15]

4:30 pm: **Organic materials for spectral hole burning and non-hole burning narrowband optical filters** *(Invited Paper)*, Anshel Gorokhovsky, College of Staten Island (USA) . . . . . [8272-16]

4:45 pm: **Sound light: rendering photoacoustics fluence-independent by adding acousto-optic modulation** *(Invited Paper)*, Wiendelt Steenbergen, Altaf Hussain, Khalid Daoudi, Univ. Twente (Netherlands) . . . . . [8223-79]

5:00 pm: **Efficient high-etendue four-wave mixing in a spectral hole-burning medium** *(Invited Paper)*, Byoung S. Ham, Inha Univ. (Korea, Republic of); Philip R. Hemmer, Texas A&M Univ. (USA). . . . . [8272-17]

5:15 pm: **Non-invasive blood flow measurements using ultrasound modulated diffused light**, Noam Racheli, Avihai Ron, Coby Metzger M.D., Ilan Breskin, Michal Balberg, Revital Shechter, Ornim Medical Ltd. (Israel) . [8223-80]

Seno Medical Best Paper Awards

Room: 305 (Esplanade) . . . . . Tues. 5:15 to 5:30 pm

Session Chairs: **Alexander A. Oraevsky,** TomoWave Labs., Inc. (USA); **Lihong V. Wang,** Washington Univ. in St. Louis (USA)

Prize donated by: **Seno Medical (USA)**

Courses of Related Interest

SC029 Tissue Optics (Jacques) Sunday, 1:30 to 5:30 pm

See Course Materials Desk located near the SPIE Registration Area, North Lobby for course and workshop details.

SPIE

2012 BiOS

SPIE Photonics West

Technical Summaries

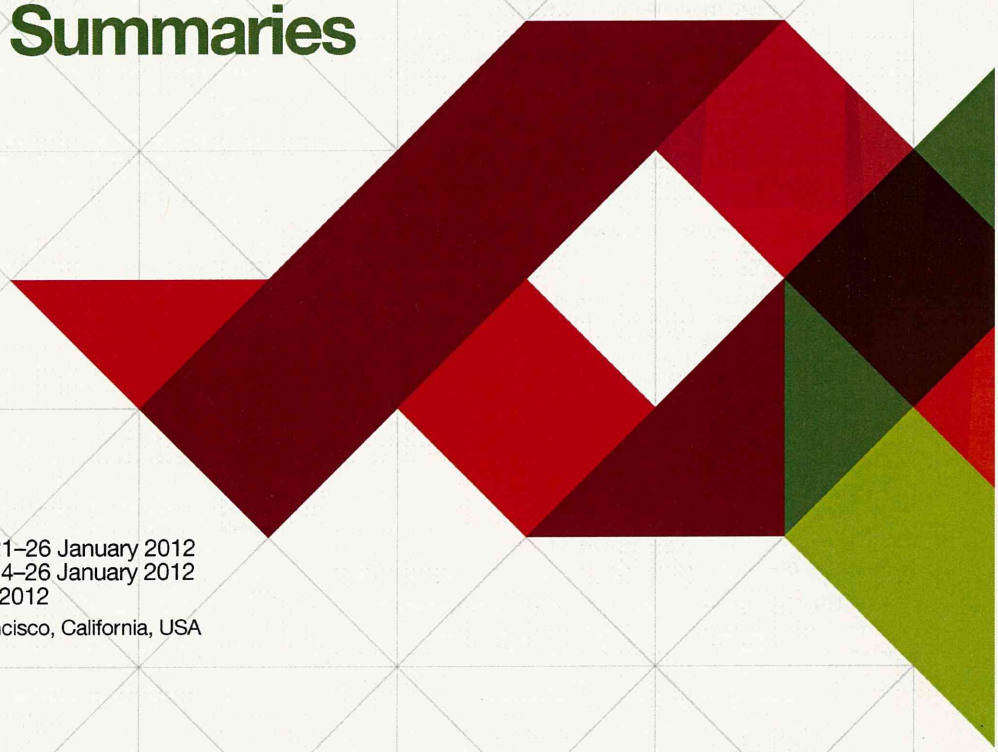

Conferences and Courses: 21–26 January 2012
Photonics West Exhibition: 24–26 January 2012
BiOS EXPO: 21–22 January 2012
The Moscone Center | San Francisco, California, USA

spie.org/pw

2012 BiOS

SPIE Photonics West

8223-101, Poster Session

DVD pickup head based optical resolution photoacoustic microscopy

P. Wang, M. Li, National Tsing Hua Univ. (Taiwan)

Optical resolution photoacoustic microscopy (OR-PAM) has been shown as a promising tool for label-free micro-vascular and single-cell imaging in clinical and bioscientific applications. However, most OR-PAM systems are realized by using a bulky laser for photoacoustic excitation. The large volume and high price of the laser may restrain the popularity of OR-PAM. In this study, we develop a low-cost and compact OR-PAM system based on a commercially available DVD pickup head. We showed that the DVD pickup head have the required laser energy and focusing optics for OR-PAM. The firmware of a DVD burner was modified to enable its laser diode to provide a 13-ns laser pulse with 1.3-nJ energy at 650 nm. Two excitation wavelengths at 650 and 780 nm were available. The laser beam was focused onto the target after passing through a 0.6-mm thick DVD transparent polycarbonate coating, and then aligned to be confocal with a 50-MHz focused ultrasonic transducer in forward mode. To keep the target on focus, a scan involving auto-tracking procedure was performed. The lateral resolution was verified via cross-sectional imaging of a 6-um carbon fiber. The measured -6 dB width of the carbon fiber was 6.66 um which was in agreement with optical diffraction limit. The proposed OR-PAM has potential as an economically viable and compact blood screening tool available outside of large laboratories due to its low cost and portability. Furthermore, a better spatial resolution could be provided by using a blue ray DVD pickup head.

8223-102, Poster Session

Influence of laser pulse width to the photoacoustic temporal waveform and the image resolution with a solid state excitation laser

K. Irisawa, K. Hirota, K. Tsujita, FUJIFILM Corp. (Japan); T. Hirasawa, M. Ishihara, National Defense Medical College (Japan)

Properties of excitation laser are the important parameters that affect the photoacoustic image quality. As for the pulse width, it is closely related to signal strength and image resolution, which reported as a result of an experiment using a laser diode that can control the pulse width relatively easily [1]. However, though a solid-state laser is promising for a medical application due to its high pulse energy creating high photo acoustic signal, its influence on waveform or the image quality has not been discussed in detail because the pulse width is hardly changeable in a solid-state laser.

We use two kinds of solid-state lasers, i.e., Q-switched Nd:YAG and Ti-Sapphire Laser, in this study and create different pulse width between 4.2ns and 45ns by changing wave length and excitation energy. These laser pulses are entered into a silicon tube composed of carbon-particle suspension as absorber whose wavelength dependence for absorption is small. We detect the generated laser-induced photoacoustic waves by hydrophone.

The photoacoustic temporal waveform shows sharper as the pulse width is shorter, which also indicates high frequency signal components increase. The width of the first peak on the temporal waveform is corresponding to the pulse width. Additionally, as a result of the photoacoustic imaging experiment preformed with 192-channel PZT linear array probe to image a thin wire, the modulated transfer function shows that the narrower the pulse width, the better the image resolution.

[1] T. J. Allen and P. C. Beard, Opt. Lett. 31, 3462-3464 (2006).

8223-103, Poster Session

New adaptive beamforming with spatially smoothed coherence factor for photoacoustic imaging

J. Kang, J. H. Chang, Y. Yoo, T. Song, Sogang Univ. (Korea, Republic of)

In photoacoustic imaging, an adaptive beamforming method with coherence factor (ABF-CF) was previously introduced for improving spatial resolution and signal-to-noise ratio (SNR) over a conventional delay-and-sum beamforming method (DAS). However, the ABF-CF method is not suitable for being used in practical diagnosis due to a significant amount of artifacts (e.g., irregular speckle patterns) caused by inter-channel interferences.

In this paper, a new adaptive beamforming method with spatial-smoothed coherence factor (ABF-SSCF) is presented for photoacoustic imaging to enhance the spatial resolution while preserving the regular speckle patterns by applying a spatial-smoothing technique into CF values from multiple sub-arrays within an array probe. To evaluate the proposed ABF-SSCF method, the in vitro experiments were conducted where 64-channel pre-beamformed radio-frequency (RF) data were captured from a 0.5-mm diameter graphite-lead-injected PVC phantom with a commercial ultrasound system equipped with a research package by using a 7-MHz linear array probe (SonixTouch, Ultrasonix Corp., BC, Canada) and an Nd:Yag laser excitation system (LS-2132U, LOTIS Ltd., Belarus).

From the in vitro experiments, the proposed ABF-SSCF method provides the 0.9-mm improvement in -20-dB lateral resolution compared to the DAS method, and this improvement is comparable to the ABF-CF method (i.e., 2.8 mm, 1.8 mm, and 1.9 mm for DAS, ABF-CF, and ABF-SSCF, respectively) while potentially avoiding image distortions in terms of a degree of preservation of the speckle patterns compared to the ABF-CF method.

These results indicate that the proposed ABF-SSCF method can effectively enhance the spatial resolution for photoacoustic imaging without artifacts such as irregular speckle patterns.

8223-104, Poster Session

Model-based image enhancement in optoacoustic tomography of the mouse brain

A. Rosenthal, T. Jetzfellner, X. L. Deán Ben, D. Razansky, V. Ntziachristos, Helmholtz Zentrum München GmbH (Germany)

In optoacoustic tomograophy, detector geometry plays an important role in determining the image quality. When image reconstruction is performed without accounting for the effect of detector geometry, the resolution of the image may be degraded. This is often the case when flat acoustic detectors with relatively large size are used. When reconstruction is performed without accounting for the geometry of these detectors, the resolution in the tangential direction is degraded.

In this work we developed a model-based reconstruction method which accounts for detector geometry. The model is composed of two steps: First, the relation between the detected signals and the optoacoustic image is discretized under the assumption of point detectors. Then, the effect of the detector is taken into account by temporally convolving its response with the signals obtained in the first step. The results are saved in a matrix which is subsequently inverted to obtain the optoacoustic image. Regularization is applied in the matrix inversion to enable stable reconstruction.

The method is demonstrated in an ex vivo experiment, where the brain of a mouse was imaged using cylindrically focused transducers. Significant resolution enhancement is obtained using the new technique as compared to the reconstruction obtained by model-based inversion that does not account for the detector geometry. In the enhanced images, the contrast of some anatomical features was increased by over a factor of 3.

8223-109, Poster Session

Continuous wavelet-transform analysis of photoacoustic signal waveform to determine optical absorption coefficient

T. Hirasawa, M. Ishihara, National Defense Medical College (Japan); K. Tsujita, K. Hirota, K. Irisawa, FUJIFILM Corp. (Japan); M. Kitagaki, M. Fujita, M. Kikuchi, National Defense Medical College (Japan)

In photo-acoustic (PA) imaging, valuable medical applications based on optical absorption spectrum such as contrast agent imaging and blood oxygen saturation measurement have been investigated. In these applications, there is an essential requirement to determine optical absorption coefficients accurately. In present, PA signal intensities have been commonly used to determine optical absorption coefficients. This method achieves practical accuracy by combining with radiative transfer analysis. However, time consumption of radiative transfer analysis and effects of signal generation efficiencies were problems of this method.

In this research, we propose a new method to determine optical absorption coefficients using continuous wavelet transform (CWT). We used CWT to estimate instantaneous frequencies of PA signals which reflects optical absorption distribution.

We demonstrated an experiment to validate the effectiveness of CWT in determination of optical absorption coefficients. In the experiment, planar shaped samples were illuminated to generate PA signal and its optical properties were adjusted by changing the concentration of dye solution. The PA signal was measured by our fabricated PA probe in which an optical fiber and a ring shaped P(VDF-TrFE) acoustic sensor were coaxially aligned. Tunable Ti:Sapphire laser (680 - 900 nm) was used as illumination source.

As a result of experiment, strong correlation between optical absorption coefficients of samples and the instantaneous frequency of PA signal obtained by CWT were confirmed. Advantages of this method were less interference of light transfer and signal generation efficiency

This work was partially supported by Health and Labour Sciences Research Grants for Research on Medical Device Development.

8223-110, Poster Session

Functional photoacoustic micro-imaging of rat cerebral hemodynamic response function in single vessels during forepaw electrical stimulation

L. Liao, National Chiao Tung Univ. (Taiwan); Y. Chen, National Yang Ming Univ. (Taiwan); C. Lin, J. Chang, National Chiao Tung Univ. (Taiwan); M. Li, National Tsing Hua Univ. (Taiwan)

The specificity of the hemodynamic response function (HRF) is determined spatially by the vascular architecture and temporally by the evolution of hemodynamic changes. Here, we used functional photoacoustic microscopy (fPAM) to investigate the spatiotemporal evolution of the HRFs of hemoglobin concentration (HbT), cerebral blood volume (CBV) and hemoglobin oxygen saturation (SO2) in single cerebral vessels to rat left-forepaw stimulation. The HRF changes in specific cerebral vessels responding to different stimulation intensities and durations were bilaterally imaged with 36 × 65-um spatial resolution. Various electrical stimulations were applied with stimulation intensities at 1, 2, 6 and 10-mA combined with 5-s and 15-s stimulation durations, respectively. Our main findings were as follows: 1) the functional HbT and SO2 increased sub-linearly (i.e. compressed) with increasing stimulus intensities; 2) the results suggested that the CBV changes are more linearly correlated with arterioles than HbT and SO2 within a limited dynamic range of stimulation intensities and duration and 3) time to the peak for HbT, CBV and SO2 was lower in the bigger arterioles than that in the smaller arterioles. The findings in this study indicate that the regulation of hemodynamic changes in single vessels can be reliable studied by the fPAM technique without the use of contrast agents.

8223-111, Poster Session

Photoacoustic array imaging of calcifications: phantom study

Y. Cheng, T. Hsiao, National Tsing Hua Univ. (Taiwan); W. Tien, S. Luo, D. Chiou, Industrial Technology Research Institute (Taiwan); M. Li, National Tsing Hua Univ. (Taiwan)

Breast calcification is one of the most important indicators for early breast cancer detection. In our previous study, we have demonstrated the feasibility of visualization of calcifications using photoacoustic microscopy setup. In this study, based on a medical ultrasound array imaging platform, we attempt to develop a real-time and high penetration photoacoustic (PA) array imaging system for visualization of breast calcifications. Phantom studies were used to verify the imaging capability and penetration depth of the developed PA array system for calcification imaging. Intralipid gelatin phantoms with different-sized hydroxyapatite (HA) particles - major chemical composition of the breast calcification associated with malignant breast cancers - embedded were imaged. Laser at 750 nm was used for photoacoustic excitation and a custom-made 5-MHz photoacoustic array transducer with linear light guides was applied for photoacoustic signal detection. To obtain better image contrast, coherence weighting was applied in addition to delay and sum beamforming. Experimental results demonstrated that this system is capable of calcification imaging of 300-500 um HA particles. For the 500-um HA particles, the imaging contrast was about 34 dB and the achievable penetration was 20 mm where the axial, lateral, and elevational resolution of this PA array imaging system is 0.39 mm, 0.38 mm, and 1.25 mm, respectively. The highest frame rate was 10 frames/sec limited by the laser pulse rate. Future work will focus on optimization of the photoacoustic transducer to further improve the penetration depth and development of photoacoustic and ultrasound dual-modal imaging to enhance the calcification imaging capability.

8223-112, Poster Session

Signal recovered from a photoacoustic imaging based on a long-focal-zone transducer

W. Xie, Z. Zeng, L. Li, Z. Li, H. Li, Fujian Normal Univ. (China)

The photoacoustic (PA) signal attenuation was affected by many factors in an imaging system. In this presentation, the factors lead to the signal attenuation and their characters were discussed based on tissue optics, acoustic transport and detection in a long-focal-zone PA imaging system. A method to recover the detected PA signals was presented and employed to image a thyroid sample in vitro. The experimental results demonstrated that the method could be used to improve the imaging depth and quality in the PA system.

Continuous wavelet-transform analysis of photo-acoustic signal waveform to determine optical absorption coefficient

T. Hirasawa[a], M. Ishihara[a], K. Tsujita[b], K. Hirota[b], K. Irisawa[b], M. Kitagaki[a], M.Fujita[c], M.Kikuchi[d]
[a] Dept. of Medical Engineering, National Defense Medical College, Japan
[b] Medical Systems Research & Development Center, Research & Development Management Headquarters, FUJIFILM Corporation, Japan
[c] Div. of Environmental Medicine, National Defense Medical College Research Institute, Japan
[d] Vice President and Dean, National Defense Medical College , Japan

ABSTRACT

In photo-acoustic (PA) imaging, valuable medical applications based on optical absorption spectrum such as contrast agent imaging and blood oxygen saturation measurement have been investigated. In these applications, there is an essential requirement to determine optical absorption coefficients accurately. In present, PA signal intensities have been commonly used to determine optical absorption coefficients. This method achieves practical accuracy by combining with radiative transfer analysis. However, time consumption of radiative transfer analysis and effects of signal generation efficiencies were problems of this method. In this research, we propose a new method to determine optical absorption coefficients using continuous wavelet transform (CWT). We used CWT to estimate instantaneous frequencies of PA signals which reflects optical absorption distribution. We validated the effectiveness of CWT in determination of optical absorption coefficients through an experiment. In the experiment, planar shaped samples were illuminated to generate PA signal. The PA signal was measured by our fabricated PA probe in which an optical fiber and a ring shaped P(VDF-TrFE) ultrasound sensor were coaxially aligned. Optical properties of samples were adjusted by changing the concentration of dye solution. Tunable Ti:Sapphire laser (690 – 1000 nm) was used as illumination source. As a result, we confirmed strong correlation between optical absorption coefficients of samples and the instantaneous frequency of PA signal obtained by CWT. Advantages of this method were less interference of light transfer and signal generation efficiency.

Keywords: photoacoustic, wavelet, acoustic frequency spectrum, optical absorption coefficient, P(VDF-TrFE)

1. INTRODUCTION

Photo-acoustic (PA) imaging is a combined technique of ultrasound and optical imaging [1]. This technique provides tomographic image of deep biological tissues beyond the limitation of optical imaging due to strong scattering. Multispectral PA imaging has been widely researched as a functional imaging technique taking advantage of optical absorption contrast [2-4]. This technique generally estimates absorption spectrums of biological tissues from spectral dependence of PA images and valuable medical applications of which such as blood oxygenation imaging [3, 4] and molecular imaging [2] were reported. In these applications, in order to identify optical absorbers and quantify their concentrations, accurate optical absorption coefficient determination methods have been required. A peak intensity of a PA signal has been used as a parameter to determine an optical absorption coefficient from a PA image because an initial pressure of PA wave is directly proportional to optical absorption distribution. Maslov et al. reported quantification of blood oxygenation in blood vessels using this parameter [3]. However, in their *in-vivo* experiment, spectral dependences of PA signals were caused by not only absorption spectrums of bloods in blood vessels but also optical attenuation in surrounding tissues . Then, the accuracy of the blood oxygenation quantification was significantly degraded. In order to compensate effects of optical attenuation, Laufer et al. calculated an optical energy distribution by solving the radiation transfer equation [4]. Compensation of optical attenuations improved the accuracy of the optical absorption coefficient determination. However, the calculation requires some assumption to obtain a unique solution and consumes times. These factors have constrained an applicability of this method.

*hirasawa@ndmc.ac.jp: phone +81 4 2995-1596; fax +81 4 2996-5199; address 3-2, Namiki, Tokorozawa, Saitama, Japan, 359-8513

Photons Plus Ultrasound: Imaging and Sensing 2012, edited by Alexander A. Oraevsky, Lihong V. Wang,
Proc. of SPIE Vol. 8223, 822333 · © 2012 SPIE · CCC code: 1605-7422/12/$18 · doi: 10.1117/12.908088

We proposed an optical absorption coefficient determination method using a temporal waveform of a PA signal. The merit of this method is reduced effect of optical attenuation. A temporal waveform of a PA signal also depends on an optical absorption coefficient because an initial pressure of a PA wave is related to an optical absorption distribution. An optical absorption distribution could be expressed as a product of an optical absorption coefficient and an energy distribution. For an optical absorber with uniform optical absorption coefficient, the optical absorption distribution is proportional to the energy distribution which attenuates exponentially with a rate of the optical absorption coefficient. The proposed method does not require absolute PA signal intensity then it is not affected by optical attenuation in surrounding tissue. However, the temporal waveform of the PA signal is strongly affected by noises due to low signal to noise ratio (SNR) of the PA signal.

In this research, in order to reduce effects of noises we focused onto frequency spectrums of PA signals. A frequency spectrum of a PA signal also reflects an optical absorption coefficient and if a principle component of an additive noise in the PA signal is a white noise, the frequency spectrum provides higher SNR than the temporal waveform because the white noise is averaged in the frequency domain. In order to obtain the time resolved frequency spectrum of the PA signal, we introduced continuous wavelet transform (CWT) [6]. One of the features of CWT is a scalable width of time window which enables both high frequency resolution in low frequency component and high temporal resolution in high frequency component.

Some groups already introduced wavelet transform to a PA signal analysis. For examples of noise reduction, J. A. Viator et al. and some groups applied discrete wavelet transform to reduce a white noise from a PA signal [7, 8]. And for an example of a waveform characterization, I. Patrikeev et al. reported correlation between CWT of a simulated PA signal and both concentration and oxygen saturation of hemoglobin [9]. However, the relationship between CWT of PA signals and optical absorption coefficients has not been reported.

We report systematical relationship between optical absorption coefficients and CWT of PA signals. In out experiment, PA signals were generated from several phantoms with different optical absorption coefficients and then measured by P(VDF-TrFE) ultrasound sensor with wide frequency band width.

2. MATERIALS AND METHOD

2.1 Principle

2.1.1 Photo-acoustic signal equation

In condition satisfying acoustically homogeneous and thermal confinement, an acoustic pressure $p(r,t)$ referred as a PA signal is expressed as a follow wave equation.

$$c^2\nabla^2 p(\boldsymbol{r},t) - \frac{\partial^2 p(r,t)}{\partial t^2} = -\frac{c^2\beta}{C_p}\frac{\partial H(r,t)}{\partial t} \qquad (1)$$

Where, c is a sound speed in medium, C_p is a specific heat at constant pressure, and β is a thermal expansion coefficient, respectively. A heat generation $H(r,t)$ caused by an absorption of excitation laser pulse is expressed as a follow equation.

$$H(\boldsymbol{r},t) = \mu_a(\boldsymbol{r}) \cdot F_o(\boldsymbol{r}) \cdot \eta(t) \qquad (2)$$

Where, $F_o(\boldsymbol{r},t)$ is a local fluence, $\eta(t)$ is a temporal waveform of an excitation laser pulse, and $\mu_a(\boldsymbol{r})$ is an optical absorption coefficient. When the condition of stress confinement is satisfied, $\eta(t)$ can be approximated as the Dirac delta function, and then follow equation can be derived from eq. (1) and eq.(2) using the Green's function expansion [1].

$$p(\boldsymbol{r},t) = \frac{\beta}{4\pi C_p}\frac{\partial}{\partial t}\left[\frac{1}{ct}\int \mu_a(\boldsymbol{r}')F_o(\boldsymbol{r}')\delta\left(t - \frac{|r-r'|}{c}\right)d\boldsymbol{r}'\right] \qquad (3)$$

Where, $\boldsymbol{r}$ is an observation point. We substituted $\boldsymbol{r} = \boldsymbol{0}$ for simplicity and introduced the spherical coordinate then a follow equation was derived.

$$p(\boldsymbol{0},t) = \frac{\beta}{4\pi C_p}\frac{\partial}{\partial t}[ct\iint \mu_a(ct,\theta,\varphi)F_o(ct,\theta,\varphi)sin\theta d\theta d\varphi] \qquad (4)$$

From eq. (4), a temporal waveform of a PA signal corresponds to differential in radial direction of an optical absorption distribution around the observation point. By using Fourier transform, a follow equation is derived.

$$\tilde{p}(\mathbf{0},k)=\frac{\beta}{4\pi C_p}ik\left[\iint\frac{\partial}{\partial k}\{\tilde{\mu}_a(k,\theta,\varphi)*\tilde{F}_o(k,\theta,\varphi)\}sin\theta d\theta d\varphi\right] \quad (5)$$

Where, $\tilde{p}(\mathbf{0},k)$, $\tilde{\mu}_a(k,\theta,\varphi)$, and $\tilde{F}_o(k,\theta,\varphi)$ are Fourier transform of $p(\mathbf{0},t)$, $\mu_a(ct,\theta,\varphi)$, and $F_o(ct,\theta,\varphi)$, respectively. A frequency f can be calculated from a wavenumber k by an equation of $f=ck$. From eq. (5), a frequency spectrum of a PA signal depends on an optical absorption distribution in an optical absorber. In the PA signal acquired using an ultrasound sensor with narrow directionality, integrals in θ,φ axis included in eq. (4) and (5) could be neglected. Further, assuming the optical absorber with homogeneous optical absorption coefficient, the temporal waveform and the frequency spectrum of the PA signal reflects an optical attenuation in the optical absorber which depends on the optical absorption coefficient.

2.1.2 Continuous wavelet transform using Mexican-hat wavelet

Continuous wavelet transform (CWT) is a time resolved frequency spectrum analysis technique. In another time resolved frequency spectrum analysis technique of short time Fourier transform, a constant width of time window results in a lack of a time resolution especially in a high frequency component. On the other hand, a scalable width time window of CWT results both high temporal resolution in high frequency component and high frequency resolution in low frequency component [6].

In CWT, daughter wavelet $\Psi_{a,b}(t)$ is expressed as a follow equation, which is shifted and scaled mother wavelet function $\Psi(t)$ with no DC component and finite time width.

$$\Psi_{a,b}(t)=\frac{1}{\sqrt{a}}\Psi\left(\frac{t-b}{a}\right) \quad (6)$$

Where, a is a scale relates to time domain expansion of wavelet function and b is a shift relates to time domain displacement of wavelet function, respectively. By increasing the scale, the temporal width of the wavelet function is expanded with keeping constant wavenumber then the frequency of the wavelet function is decreased. Conversely, by decreasing the scale, the frequency of the wavelet function is increased. The CWT calculates the wavelet transform $\mathrm{T}(a,b)$ of the PA signal $x(t)$, from a follow convolution integral of the PA signal $x(t)$ and the daughter wavelet $\Psi_{a,b}(t)$.

$$\mathrm{T}(a,b)=\int_{-\infty}^{\infty}x(t)\,\Psi_{a,b}{}^{*}(t)dt \quad (7)$$

Where, $\Psi_{a,b}{}^{*}(t)$ is the complex conjugate of $\Psi_{a,b}(t)$. Since the scale and the shift of the wavelet transform can be converted to a frequency and a time, wavelet transform is equivalent to time resolved frequency spectrum analysis of a signal.

We adopted the Mexican-hat wavelet as the mother wavelet of CWT. This wavelet provides high temporal resolution comparing to other wavelets. This wavelet is second order differential of the Gaussian function which is expressed as follow equation.

$$\Psi(t)=(1-t^2)e^{-\frac{t^2}{2}} \quad (8)$$

The central frequency of this wavelet is $f_0=\sqrt{2}/2\pi$ and the central frequency of daughter wavelets $\Psi_{a,b}(t)$ could be expressed as $f=f_0/a$. We defined central frequencies of wavelets as pseudo frequencies.

2.2 PA signal measurement using phantom

In order to confirm relationship between CWT of PA signals and optical absorption coefficients of optical absorbers, we measured PA signal using phantoms. The phantoms consisted of two layers, the upper was a turbid layer which simulated optical attenuation due to optical scattering and the lower was an absorption layer which simulated optical absorption in optical absorber and generated PA wave. Both layers contain 1.5 wt% of agar and had thickness of 9.5 mm. Upper layers contain 0, 1.16, 2.33, 4.67 vt% of intralipos (Otsuka Pharmaceutical) as optical scatterers. The 4.67 vt% intralipos had the reduced scattering coefficient of $\mu_s'=10\mathrm{cm}^{-1}$ which was nearly equal to that of a muscle tissue [10, 11]. Lowers layer contain 1, 2, 4, 8, 16, 32 vt% of black ink (BI) as optical absorbers. The 1 vt% BI had the absorption coefficient of $\mu_a=2.82\ cm^{-1}$ for the wavelength of 720 nm.

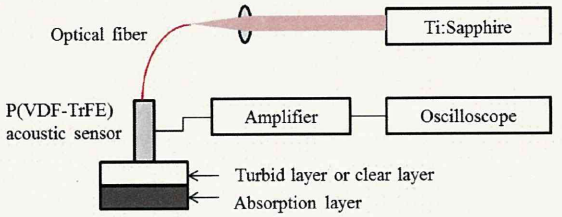

Fig.1 Schematic diagram of an experimental setup

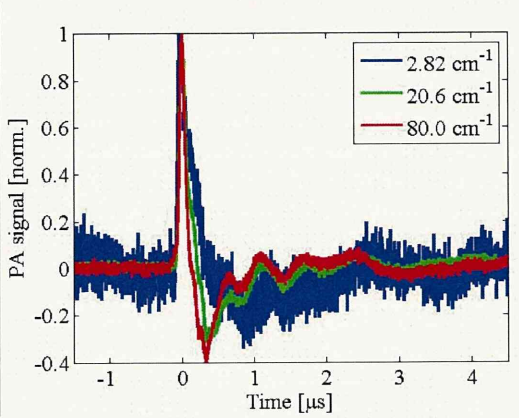

Fig. 2 Temporal waveform of PA signal generated from absorption layer with various concentrations of black ink. Amplitude of PA signal is normalized to have peak intensity of 1. The waveforms were shifted in time domain to have peak intensities at 0 μs.

Schematic diagram of the experimental setup is shown on fig.1. A Tunable Ti:Sapphire laser (LT2242, Lotis:Tii) pumped by second harmonic of Q-switched Nd:YAG laser was used to generate excitation laser pulse. The wavelength of the laser pulse was tuned to 720 nm. This wavelength of light penetrates relatively deeply into biological tissues. The excitation laser pulse with a width of 15ns was irradiated to phantoms via an optical fiber with a core diameter of 400 μm and a numerical aperture of 0.48. In order to prevent saturation of a detection system described below, the pulse energy of the laser pulse was attenuated by ND filters before fiber coupling.

Since frequency spectrums of PA signals expressed as eq.(5) depends on optical absorption coefficients of phantoms and generally has wide frequency band width, an ultrasound sensor with a wide frequency band width is required. Then, we used our originally designed ultrasound sensor made of piezoelectric polymer P(VDF-TrFE) to detect the PA signal. The piezoelectric film P(VDF-TrFE) has relatively wide frequency band width than conventional ultrasound sensors made of piezoelectric ceramic PZT. The ring shaped detection element of the sensor had an inner diameter of 0.6mm and an outer diameter of 4.0 mm respectively. By passing the optical fiber into the hole of the ring shaped element, the optical excitation axis and the ultrasound detection axis were aligned coaxially.

PA signals generated from phantoms were measured by contacting the ultrasound sensor to phantoms surfaces via optical transparent acoustic coupling gel (UF clear gel, FUKUDA-Denshi). The PA signal detected by the ultrasound sensor is amplified by a FET amplifier (SA-220F5, NF Electronic Instruments, 46 dB, 0.1 – 80 MHz) and then, memorized by a digital oscilloscope (DSO8104A, Agilent, 4 GSa/s).

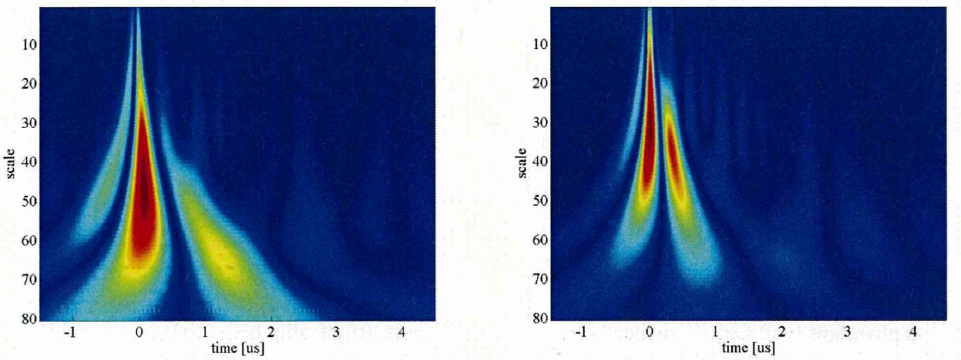

(a) μ_a =2.82 cm^{-1} (b) μ_a =80.0 cm^{-1}

Fig. 3 Scalograms of photo-acoustic signals obtained using Mexican hat wavelet transform.

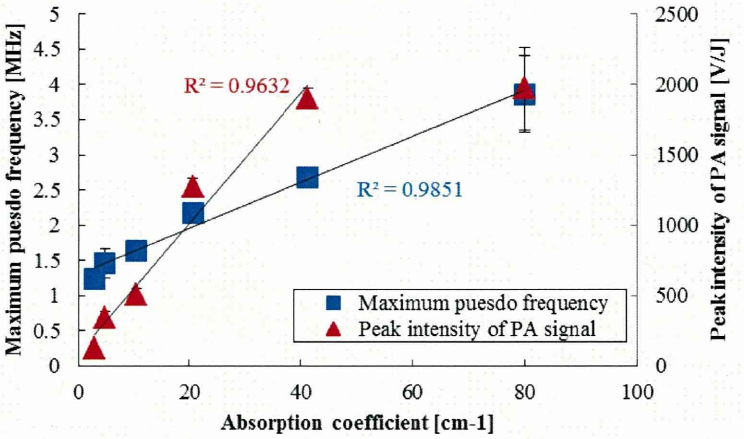

Fig.4 Relationship between optical absorption coefficients and maximum pseudo frequency or PA signals intensity. Maximum pseudo frequency is calculated from wavelet scale with largest wavelet coefficient. The error bar expresses standard deviation of measurements with N=4.

3. RESULTS AND DISCUSSION

Temporal waveforms of PA signals generated from absorption layers with absorption coefficients of 2.82 cm^{-1} and 80.0 cm^{-1} placed under a clear layer is shown on fig.2. In order to compare waveforms of PA signals, voltages of each PA signals were normalized to have maximum intensities of 1. Fig.3 shows results of CWT for PA signals generated from absorption layers with absorption coefficients of 2.82 cm^{-1} and 80.0 cm^{-1}. Images shown on fig.3 were referred as scalograms which expresses intensities of CWT $T(a, b)$. The vertical axis of a scalogram is scale a and the other axis is shift b, and these parameters relate to frequency and time respectively. By comparing scalograms shown on fig.3, the PA signal generated from the phantom with the absorption coefficient of 80.0 cm^{-1} had strong peak at lower scale (high frequency) component. Then we used maximum pseudo frequency as a parameter to determine optical absorption coefficient. Maximum pseudo frequency was converted from the scale value. Fig.4 shows relationship between maximum pseudo frequency and optical absorption coefficient. Maximum intensities of PA signals were also plotted on fig.4, which were commonly used to determine optical absorption coefficient.

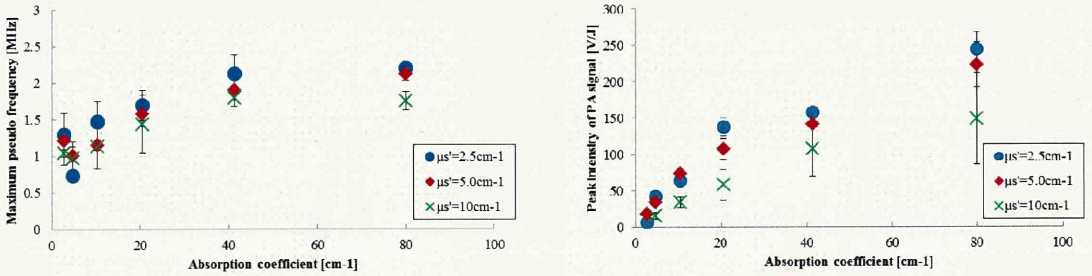

Fig.5 Left: Relationship between Maximum pseudo frequency and absorption coefficient of optical absorber placed under the turbid phantoms with various reduced scattering coefficients. Right: ship between peak intensity of PA signal and absorption coefficient of optical absorber placed under the turbid phantoms with various reduced scattering coefficients. The error bar expresses standard deviation of measurements with N=4.

As shown on fig.4, both peak intensities and maximum pseudo frequencies had linear relationship with optical absorption coefficients. However, at range of optical absorption coefficients greater than 40 cm^{-1}, the increase of peak intensities were saturated. On the other hand, maximum pseudo frequency kept linearity through optical absorption coefficient range measured in this experiment and correlation coefficient was 0.985. Maximum pseudo frequencies at absorption coefficients of 10 – 80 cm^{-1} were dominant factor to increase correlation coefficient then, by focusing onto absorption coefficients of 1 – 10 cm^{-1}, correlation coefficient decreased to 0.887. Then, linearity in lower absorption coefficient range was one of the challenges of this method.

In order to validate effects of optical scattering of biological tissues, turbid layers were placed onto absorption layers and then PA signal was measured. The measured PA signal was analyzed by using CWT. Fig.5 shows maximum pseudo frequencies and PA signal intensities respectively. As shown in fig.5, maximum pseudo frequencies increased with optical absorption coefficients however, pseudo frequencies of PA signals shown in fig.5 were lower than that of fig.3. For example, in case of the absorption coefficient is 80.0 cm^{-1}, the maximum pseudo frequency was decreased from 3.86 MHz to 1.79 MHz.

This effect could be prevented by focusing the sensitive area of the ultrasound sensor because this effect was caused by spatial expansion of the optical absorption area at the surface of absorption layer due to optical diffusion in the turbid layer. The ultrasound sensor used in this experiment had narrow directionality and approximately 4mm diameter sensitive area on the surface of absorption layer. Then, temporal expansion of PA signal could be calculated as 308 ns from the sensitive area of ultrasound sensor and the distance between the ultrasound sensor and the absorption layer. This calculated temporal expansion of the PA signal almost coincided with the decrease of the maximum pseudo frequency. Then, the decrease of maximum pseudo frequency was caused by expansion of optical absorption area on the surface of absorption layer. By focusing the sensitive area of ultrasound sensor, the sensor will not sense the PA signal induced at expanded area then, the effect of optical diffusion could be reduced. However, optical scattering and thickness of samples may suffer optical penetration depth especially for optical absorber with low absorption coefficient then, further discussion is required.

On the other hand, maximum intensities of PA signals were decreased by increasing optical scattering coefficients. In case of the absorption coefficient is 80.0 cm^{-1}, peak intensity decreased 1970.5 V/J to 148.6 V/J due to optical scattering. Then, in order to estimate optical absorption coefficient of absorption layer from maximum intensity of PA signal, optical attenuation should be compensated. So, optical absorption coefficient determination using CWT have potential to be the alternative method.

4. CONCLUSION

We proposed an optical absorption coefficient determination method using CWT which does not require optical energy distribution compensation because it was less affected by optical attenuation. We defined the parameter maximum pseudo frequency to determine optical absorption coefficient. The parameter was calculated from the scale with maximum intensity in CWT of PA the signal. We measured PA signal using phantom in order to confirm the correlation between optical absorption coefficients and maximum pseudo frequencies. As results, maximum pseudo frequencies had linear relationship with optical absorption coefficients through a wider range of absorption coefficients comparing to peak intensity of PA signal. However, by placing optical scatterer between sensor and absorption layer, frequency of PA signal was decreased. This effect was caused by expansion of optical absorption area on the surface of absorption layer and which could be prevented by focusing sensitive area of ultrasound sensor. Then, CWT has potential as an alternative optical absorption coefficient determination method.

5. ACKNOWLEDGEMENTS

This work has been partially supported by Health and Labour Sciences Research Grants for Research on Medical Device Development, and Magnetic Health Science Foundation. Authors appreciate the important contribution for this study with Mr. K. Hirota and Mr. T. Abe(FUJIFILM Corp.). Authors thank Ms. M. Tanikawa and Ms. Y. Mayumi for their contributions for experiment. Experiments were also supported by Laboratory Center, National Defense Medical College and Center for Laboratory Animal Experiment, National Defense Medical College.

REFERENCES

[1] Li, C., and Wang, L. V., "Photoacoustic tomography and sensing in biomedicine", Phys. Med. Biol., 54, R59-R97 (2009)

[2] Zerda, A., Liu, Z., Bodapati, S., Teed, R., Vaithilingam, S., Khuri-Yakub, B. T., Chen, X., Dai., H., and Gamchir, S. S., "Ultrahigh sensitivity carbon nanotube agents for photoacoustic molecular imaging in living mice", Nano Lett., 10, 2168-2172 (2010)

[3] Sivaramakrishnan, M., Maslov, K., Zhang, H. F., Stica, G., and Wang, L. V., "Limitaitons of quantitative photoacousitc measurement of blood oxygenation in small vessels", Phys. Med. Biol., 52, 1349-1361 (2007)

[4] Laufer, J., Delpy, D., Elwell, C., and Beard, P., "Quantitative spatially resolved measurement of tissue chromophore concentrations using photoacoustic spectroscopy : application to the measurement of blood oxygenation and hemoglobin concentration", Phys. Med. Biol., 52, 141-168 (2007)

[5] Ishihara, M., Hirasawa, T., Tsujita, K., Kitagaki, M., Bansaku, I., Fujita, M., and Kikuchi, M., "Multifunctional photoacoustic signals detected by P(VDF-TrFE) film sensor with a wide range of frequency", Proc. of SPIE, 7899, 78992Z-1 - 78992Z-5 (2011)

[6] Addison, P. S., "The illustrated wavelet transform handbook introductory theory and applications in science, engineering, medicine and finance", IOP Publishing, England (2002)

[7] Patrikeev, I., Brecht, H. –P., Petrov, Y. Y., Petrova, I. Y., Prough, D. S., and Esenaliev, R. O., "Wavelet differentiation of optoacoustic signals for monitoring of total hemoglobin concentration and oxygen satulation level in small blood vessels", Proc. of SPIE, 6437, 643717-1 – 643717-6 (2007)

[8] Holan, S. H., and Viator, J. A., "Automated wavelet denoising of photoacoustic signals for circulating melanoma cell detection and burn image reconstruction", Phys. Med. Biol., 53, N227-N236 (2008)

[9] Lu, T., Jiang, J., Su, Y., Song, Z., Yao, J., and Wang, R. K., "Signal processing using wavelet transform in photoacoustic tomography", Proc. of SPIE, 6439, 64390L-1 – 64390L-6 (2007)

[10] Staveren, H. J., Moes, C. J. M., Marle, J., Prahl, S. A., and Gemert, M. J. C., "Light scattering in intralipid-10% in the wavelength range of 400-1100nm", Applied Optics, 30(31), 4507-4514 (1991)

[11] Wang, L. V., Wu, H., [Biomedical Optics : Principles and Imaging], Wiley-interscience, Hoboken, 343 (2007)

Influence of laser pulse width to the photoacoustic temporal waveform and the image resolution with a solid-state excitation laser

K. Irisawa*[a], T. Hirasawa[b], K. Hirota[a], K. Tsujita[a], and M. Ishihara[b]
[a] Medical Systems Research & Development Center, Research & Development Management Headquarters, FUJIFILM Corporation, 798 Miyanodai, Kaisei-machi, Ashigarakami-gun, Kanagawa, Japan 258-8538;
[b] Department of Medical Engineering, National Defense Medical College, 3-2, Namiki, Tokorozawa, Saitama, Japan 359-8513

ABSTRACT

Properties of excitation laser are the important parameters that affect the photoacoustic image quality. As for the pulse width, it is closely related to signal strength and image resolution, which reported as a result of an experiment using a laser diode that can control the pulse width easily[1]. However, though a solid-state laser is promising for a medical application due to its high pulse energy creating high photo acoustic signal, its influence on waveform or the image quality has not been discussed in detail because the pulse width is hardly changeable in a solid-state laser.

We use two kinds of solid-state lasers, i.e., Q-switched Nd:YAG and Ti-Sapphire Laser, in this study and generate different pulse width between 4.5 and 45 ns by changing wavelength and excitation energy. These laser pulses are entered into a silicon tube composed of carbon-particle suspension as absorber whose wavelength dependence for absorption is small. We detect the generated laser-induced photoacoustic waves by hydrophone.

The photoacoustic temporal waveform shows sharper as the pulse width is shorter, which also indicates high frequency signal components increase. The width of the first peak on the temporal waveform is corresponding to the pulse width. Additionally, as a result of the photoacoustic imaging experiment preformed with 192-channel PZT linear array probe to image a thin wire, the modulation transfer function shows that the narrower the pulse width, the slightly better the image resolution.

Keywords: Solid-state laser, pulse width, photoacoustic waveform, photoacoustic imaging

1. INTRODUCTION

Photo-acoustic imaging is a method for acquiring image by detecting the acoustic wave when pulsed light is incident on the light absorber.[2] The resolution performance in photoacoustic image can be better than that in optical image for the light absorber that exists in the relatively deep part of scattering objects. And also the resolution performance can be higher performed by photoacoustic imaging than by ultrasound in the imaging object that reflexes the acoustic wave and absorbs the light either.[3]
By utilizing this feature, photoacoustic imaging is promising as a functional imaging modality for clinical use in recent years. For example, Hemoglobin is a representative object in the blood that can absorb the light in living organisms, and by using photoacoustic imaging, tumors accompanied with neovascularity can be observed.[4] And by injecting the contrast medium such as pigments, the imaging of lymph vessels and lymph nodes can be observed as well.[5]

In the living organism, where is the main imaging target of photoacoustic imaging, the optical wavelengths that reachable to the depths almost without absorption is limited in the range between 650 to 1100 nm. Since the light is strongly scattered in living organism, it shall reduce significantly until it reaches the depth of body. Additionally, the conversion efficiency from optical energy to acoustic energy is low. Therefore, the high-energy pulsed light source and high-sensitivity ultrasound detector are needed for practical use.

When irradiating the pulsed light with energy density of ~20 mJ/cm^2 close to the maximum permissive exposure for the human skin and with a field of view ~1cm^2 suitable for imaging of human body, the light source is needed for producing the energy pulse higher than 20 mJ/pulse.

*kaku.irisawa@fujifilm.co.jp; phone +81 465 85-4189; fax +81 465 85-2119

Photons Plus Ultrasound: Imaging and Sensing 2012, edited by Alexander A. Oraevsky, Lihong V. Wang,
Proc. of SPIE Vol. 8223, 82232W · © 2012 SPIE · CCC code: 1605-7422/12/$18 · doi: 10.1117/12.907714

In current technology, the most practicable light source is solid-state pulse laser. With the view of determining system performance, pulse width and repetitive performance, etc. other than high energy become important when using the light source of pulse laser. As for laser pulse width, it is limited and almost fixed by properties of laser crystal, and arrangement of optical elements; it is a difficult parameter to be independently designed. Therefore, it is important to study the laser pulse width dependence of photoacoustic wave, and the effect to the image quality when uses it in imaging.

In recent years, the attempt to control the pulse width in laser diode is reported, resulting in the increase of the photoacoustic signal with the decrease of the pulse width, and the significant image blurring in the pulse width about 500 ns.[1]

The purpose of this report is to clear how much the photo-acoustic image quality is dependent on the pulse width of solid-state laser. First, it is observed the temporal waveform of photoacoustic pressure by single hydrophone with the varieties of the pulse width of excitation solid-state lasers in the range of 4.5 to 45 ns for evaluating the change of temporal waveform of photoacoustic signal depending on the pulse width in detail. Then, it is compared the temporal waveform between the experimental results and the result obtained by simplified superposition model calculation.

In addition, we acquired the photoacoustic image by using ultrasound probe array at various pulse widths to study the relations between the pulse width and image quality of photoacoustic imaging system based on US imaging systems. Finally, we evaluated the image resolution to be compared with an image resolution expected from above simplified superposition model calculations.

2. MATERIALS AND METHODS

2.1 Observation of photoacoustic temporal waveform detection

In order to generating photoacoustic wave by different laser pulse widths between 4.5 and 45ns, two kinds of Q-switched solid-state lasers are used as pulsed light source, that is, a Nd:YAG second harmonic generation (SHG) laser (ML-II, Minilite, Continuum Inc, USA) and a Ti-Sapphire laser (LS-2134 and LT-2211, LOTIS TII, Belarus) in which the pulse width is changed accompanied by selecting wavelength. The pulse width and wavelength from Nd:YAG SHG laser were 4.5 ns and 532 nm, respectively. In the Ti-Sapphire laser units, the pulse widths were from 14 to 45 ns at selected wavelengths from 710 to 695 nm, respectively. The laser pulse waveforms were observed by photodiode (ET-2000, Electro-Optics Technology Inc., USA), and pulse width is defined as the full width of half maximum of the pulse waveforms. The pulse energy was set around 3 mJ. Laser light is introduced via optical fiber with 600 um core diameter. As a absorber for exciting photoacoustic pressure wave, it was used a silicon tube with 0.3 and 0.4 mm inner and outer diameter, respectively, including carbon-particle suspended in water. Though the absorption of the carbon-particle suspension is changed by the wavelength change, its absorption change is relatively small by a factor of around 0.7 in the range of wavelength from 532 to 720 nm as shown in the inset of figure 1(a). The mean diameter of carbon particles in water suspension was 200 nm.

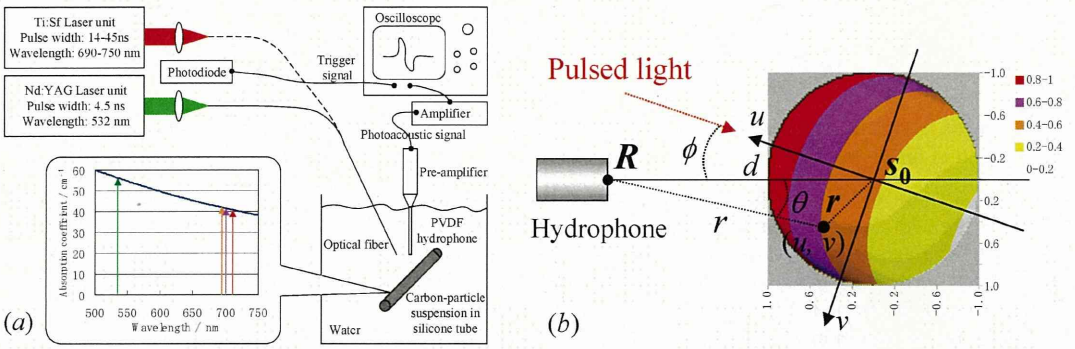

FIG. 1. (a) Experimental set up for observing photoacoustic waveforms. The inset shows the wavelength dependence of absorption coefficient for carbon-particle suspension, together with the wavelength used to change pulse width.

FIG. 1. (b) Relation between the coordinates systems used in calculation model and an example of absorption distribution A calculated with the parameters, a = 0.3 mm, d = 5.0 mm, r_P = 1.0 mm, μ = 5.62 cm^{-1}, ϕ = 25 deg.

Photoacoustic wave is detected by PVDF needle hydrophone (HPM02/1, Precision Acoustics Ltd., UK) with 0.2 mm element diameter and observed by oscilloscope. The angle between the PVDF needle hydrophone and laser incident direction was 25 degrees. The distance between silicon tube and hydrophone is set to 5 mm.

2.2 Theoretical model and numerical calculation of photoacoustic temporal waveform

The simple calculation model is introduced to consider the influence of pulse width and absorption distribution change simultaneously caused by wavelength change of laser pulse. The photoacoustic wave generated from the tube is calculated as a superposition of the spherical photoacoustic wave that generated from the individual carbon-particle of different spatial location with considering the concentration distribution of carbon-particle and distribution of incident light.

The reached photoacoustic pressure $p_{micro}(\boldsymbol{R}, t)$ in observation point $\boldsymbol{R}$ on time t from a microparticle located in $\boldsymbol{r}$ is obtained as spherical wave proportional to the temporal differential waveform of light pulse, and expressed as,[6, 7]

$$p_{micro}(\boldsymbol{R},t) = \frac{k}{|\boldsymbol{r}-\boldsymbol{R}|}\frac{d}{d(t-\frac{|\boldsymbol{r}-\boldsymbol{R}|}{v_s})} I(t-\frac{|\boldsymbol{r}-\boldsymbol{R}|}{v_s}) \quad (1).$$

Where, I is the temporal waveform of intensity of excitation laser pulse, and k is the coefficient related with conversion efficiency from the laser pulse to acoustic wave, and v_s is the sound speed. Such expression is considered to be satisfied in the case of certain particle that arises uniform thermal expansion derived from uniform absorption distribution or momentary heat diffusion in the particle. The carbon-particle with 200 nm of mean hydrodynamic diameter is used in the experiment, which is also assumed to be satisfied as the below expression.

Then, the pressure waveform $p_{macro}(\boldsymbol{R}, t)$ from the carbon-particle suspension inside the tube is assumed to be formed as superposed waveform of p_{micro} from each particle in different locations. The absorption distribution of carbon-particle suspension is defined as $A(\boldsymbol{r}-\boldsymbol{R})$. Therefore, $p_{macro}(\boldsymbol{R}, t)$ is expressed as below.[8]

$$\begin{aligned} p_{macro}(\boldsymbol{R},t) &= \iiint A(\boldsymbol{r}-\boldsymbol{R}) \times \frac{k}{|\boldsymbol{r}-\boldsymbol{R}|}\frac{d}{d(t-\frac{|\boldsymbol{r}-\boldsymbol{R}|}{v_s})} I(t-\frac{|\boldsymbol{r}-\boldsymbol{R}|}{v_s}) dV \\ &= \int_0^{\pi}\int_{-\frac{\pi}{2}}^{\frac{\pi}{2}}\int_0^{|\boldsymbol{r}-\boldsymbol{R}|=v_s t} \frac{kA(\boldsymbol{r}-\boldsymbol{R})}{|\boldsymbol{r}-\boldsymbol{R}|} I'(t-\frac{|\boldsymbol{r}-\boldsymbol{R}|}{v_s})|\boldsymbol{r}-\boldsymbol{R}|^2 \sin\theta d|\boldsymbol{r}-\boldsymbol{R}| d\theta d\varphi \\ &= \int_0^{|\boldsymbol{r}-\boldsymbol{R}|=v_s t} \frac{k}{|\boldsymbol{r}-\boldsymbol{R}|}\int_0^{\pi}\int_{-\frac{\pi}{2}}^{\frac{\pi}{2}} A(\boldsymbol{r}-\boldsymbol{R})dS \times I'(t-\frac{|\boldsymbol{r}-\boldsymbol{R}|}{v_s}) d|\boldsymbol{r}-\boldsymbol{R}| \\ &= \left[\frac{k}{|\boldsymbol{r}-\boldsymbol{R}|}\int_0^{\pi}\int_{-\frac{\pi}{2}}^{\frac{\pi}{2}} A(\boldsymbol{r}-\boldsymbol{R})dS\right] * \left[I'(t-\frac{|\boldsymbol{r}-\boldsymbol{R}|}{v_s})\right] \end{aligned} \quad (2)$$

That is, the observed pressure waveform can be expressed by the convolution of integrated $A(\boldsymbol{r}-\boldsymbol{R})$ and temporal differentiation of pulse intensity.

$A(\boldsymbol{r}-\boldsymbol{R})$ is a function of incident light and absorber distribution. In the present model, it is assumed that the light is collimated light with Gaussian spatial distribution, and the concentration of carbon-particle inside of the tube is uniform, as well as the exponential decay of light intensity from the incident interface between the tube and the suspension to the traveling direction on each cross-section of the tube. For convenience of calculation, $A(\boldsymbol{r}-\boldsymbol{R})$ is calculated according the positional coordinates (u, v, w) whose origin is set at the tube center $\boldsymbol{s}_0$. The direction of u and w are corresponded with the light incident direction and a longitudinal direction, respectively. The angle ϕ between u direction and observation direction $(\boldsymbol{s}_0-\boldsymbol{R})$, tube radius a, the distance d between the tube center and detector, and absorption coefficient μ of carbon-particle suspension is variable, which are determined from the experimental arrangement or condition. The coordinate conversion between (r, φ, θ) and $(u, v, w)$was driven as a below expression (3), and A(u, v, w) is given as expression (4). And also, an example of calculation result of A(u, v, w) is shown in figure 1(b).

$$\begin{pmatrix} u \\ v \\ w \end{pmatrix} = R(-\phi)\cdot\{(\boldsymbol{r}-\boldsymbol{R})-\boldsymbol{s}_0+\boldsymbol{R}\} = \begin{pmatrix} \cos\phi & \sin\phi & 0 \\ -\sin\phi & \cos\phi & 0 \\ 0 & 0 & 1 \end{pmatrix}\begin{pmatrix} d-r\cos\theta\cos\varphi \\ -r\sin\theta \\ r\cos\theta\sin\varphi \end{pmatrix} \quad (3)$$

$$A(u,v,w) = \exp\left\{-\mu\left(\sqrt{a^2-v^2}-u\right)\right\}\cdot\exp\left(-\frac{2\left(v^2+w^2\right)}{r_p^{\,2}}\right), u^2+v^2 \le a^2 \quad (4)$$

From these expressions, the temporal photoacoustic waveforms generated by laser pulse with various pulse widths were calculated. In the calculation, laser pulse waveform $I(t)$ was assumed to be a Gaussian function, and its full width of half maximum was defined as pulse width.

In addition to obtain the calculated temporal waveform after the hydrophone detection, the frequency components of the calculated temporal waveform was multiplied by the frequency response of hydrophone based on its calibration data and specifications (+/-4 dB < 35 MHz), followed by computing the inverse Fourier transform.

2.3 Evaluation of photoacoustic image acquired with ultrasound array probe

In order to discuss the influence of pulse width on image quality, photoacoustic images of thin carbon wire were acquired by using practical ultrasound array probe at various laser pulse widths. Then, Modulation Transfer Function (*MTF*) that is one of the evaluation indexes of image resolution was computed from each PA image.

The same solid-state lasers mentioned in 2.1 section were used as pulsed light sources. Pulse laser light was transferred by optical fiber for illuminating the thin 0.124 mm diameter carbon wire. The carbon wire was perpendicularly arranged with array direction of the array probe. The photoacoustic wave was detected by the array probe which was constructed of 192 channels of PZT transducers with 0.3 mm channel pitch. The center frequency of transducers was 8 MHz. Output signals of transducers were A/D converted with 25 ns sampling interval, and preprocessed in PAI system[2]. The images were acquired in each 0.02 mm movement of the array probe for sampling more finely than channel pitch, by using motorized stage scanning parallel to the array direction. After reconstructing the photoacoustic image by Fourier transform algorism,[8] followed by obtaining the amplitude signal by Hilbert transformation, the two-dimensional point spread function was obtained. *MTF*s of the array and depth directions were computed from the point spread functions by Fourier transform of data line along the array and time directions, respectively.

3. RESULTS AND DISCUSSIONS

3.1 Comparison of temporal waveforms between experiment and calculation

In figure 2 (*a*), it is shown that the photoacoustic signal waveforms detected with the needle hydrophone for a above mentioned tube phantom at various excitation laser pulse width from 4.5 to 45 ns, which are normalized at positive peaks. In each waveform, a strong positive peak appears initially, and then the broad negative peak appears. The time interval between positive and negative peak in each waveform is about 200 ns, which are in accordance with the inner tube diameter of 0.3 mm considering the sound speed of 1500 m/s. It is observed that the widths of positive peak increases and the negative peak become strong with increasing the laser pulse width. In figure 2 (*b*), the frequency spectra of the photoacoustic waveforms at various excitation laser pulse width is shown, which are normalized at in the frequency of 2 MHz. For each spectrum, the amplitude value is gradually decreased as frequency increases. The high-frequency components become large with narrowing laser pulse, and the signal remains up to 40 MHz in 4.5 ns pulse width.

To compare between the experimental and model calculated photoacoustic waveform, calculation results of photoacoustic temporal waveform before (as-reached) and after hydrophone detection are shown in figure 3 (*a*) and (*b*), respectively. The shape and the pulse width dependence of calculated waveforms before the hydrophone detection exhibit almost the same tendency according to the experimental waveforms. Furthermore, the calculated waveforms are broadened by considering the hydrophone detection, and demonstrate more close similarities to experimental waveforms.

The similar waveforms were obtained from both experiment and calculation, indicating that the influence of excitation-laser pulse width on photoacoustic signal is almost be able to explained on the basis of the simple model, that is, the